CCSDS Historical Document

This document's Historical status indicates that it is no longer current. It has either been replaced by a newer issue or withdrawn because it was deemed obsolete. Current CCSDS publications are maintained at the following location:

http://public.ccsds.org/publications/

The Consultative Committee for Space Data Systems

Report Concerning Space Data System Standards

PSEUDO-NOISE (PN) RANGING SYSTEMS

INFORMATIONAL REPORT

CCSDS 414.0-G-1

GREEN BOOK

March 2010

CCSDS HISTORICAL DOCUMENT

The Consultative Committee for Space Data Systems

Report Concerning Space Data System Standards

PSEUDO-NOISE (PN) RANGING SYSTEMS

INFORMATIONAL REPORT

CCSDS 414.0-G-1

GREEN BOOK

March 2010

AUTHORITY

Issue:	Informational Report, Issue 1
Date:	March 2010
Location:	Washington, DC, USA

This document has been approved for publication by the Management Council of the Consultative Committee for Space Data Systems (CCSDS) and reflects the consensus of technical panel experts from CCSDS Member Agencies. The procedure for review and authorization of CCSDS Reports is detailed in the *Procedures Manual for the Consultative Committee for Space Data Systems*.

This document is published and maintained by:

CCSDS Secretariat
Space Communications and Navigation Office, 7L70
Space Operations Mission Directorate
NASA Headquarters
Washington, DC 20546-0001, USA

FOREWORD

Through the process of normal evolution, it is expected that expansion, deletion, or modification of this document may occur. This Report is therefore subject to CCSDS document management and change control procedures, which are defined in the *Procedures Manual for the Consultative Committee for Space Data Systems*. Current versions of CCSDS documents are maintained at the CCSDS Web site:

http://www.ccsds.org/

Questions relating to the contents or status of this document should be addressed to the CCSDS Secretariat at the address indicated on page i.

At time of publication, the active Member and Observer Agencies of the CCSDS were:

Member Agencies

- Agenzia Spaziale Italiana (ASI)/Italy.
- British National Space Centre (BNSC)/United Kingdom.
- Canadian Space Agency (CSA)/Canada.
- Centre National d'Etudes Spatiales (CNES)/France.
- China National Space Administration (CNSA)/People's Republic of China.
- Deutsches Zentrum für Luft- und Raumfahrt e.V. (DLR)/Germany.
- European Space Agency (ESA)/Europe.
- Russian Federal Space Agency (RFSA)/Russian Federation.
- Instituto Nacional de Pesquisas Espaciais (INPE)/Brazil.
- Japan Aerospace Exploration Agency (JAXA)/Japan.
- National Aeronautics and Space Administration (NASA)/USA.

Observer Agencies

- Austrian Space Agency (ASA)/Austria.
- Belgian Federal Science Policy Office (BFSPO)/Belgium.
- Central Research Institute of Machine Building (TsNIIMash)/Russian Federation.
- Centro Tecnico Aeroespacial (CTA)/Brazil.
- Chinese Academy of Sciences (CAS)/China.
- Chinese Academy of Space Technology (CAST)/China.
- Commonwealth Scientific and Industrial Research Organization (CSIRO)/Australia.
- CSIR Satellite Applications Centre (CSIR)/Republic of South Africa.
- Danish National Space Center (DNSC)/Denmark.
- European Organization for the Exploitation of Meteorological Satellites (EUMETSAT)/Europe.
- European Telecommunications Satellite Organization (EUTELSAT)/Europe.
- Geo-Informatics and Space Technology Development Agency (GISTDA)/Thailand.
- Hellenic National Space Committee (HNSC)/Greece.
- Indian Space Research Organization (ISRO)/India.
- Institute of Space Research (IKI)/Russian Federation.
- KFKI Research Institute for Particle & Nuclear Physics (KFKI)/Hungary.
- Korea Aerospace Research Institute (KARI)/Korea.
- Ministry of Communications (MOC)/Israel.
- National Institute of Information and Communications Technology (NICT)/Japan.
- National Oceanic and Atmospheric Administration (NOAA)/USA.
- National Space Organization (NSPO)/Chinese Taipei.
- Naval Center for Space Technology (NCST)/USA.
- Scientific and Technological Research Council of Turkey (TUBITAK)/Turkey.
- Space and Upper Atmosphere Research Commission (SUPARCO)/Pakistan.
- Swedish Space Corporation (SSC)/Sweden.
- United States Geological Survey (USGS)/USA.

DOCUMENT CONTROL

Document	Title	Date	Status
CCSDS 414.0-G-1	Pseudo-Noise (PN) Ranging Systems, Informational Report, Issue 1	March 2010	Original issue

CONTENTS

CONTENTS (continued)

Figure Page

Table

CONTENTS (continued)

Table Page

1 INTRODUCTION

1.1 PURPOSE AND SCOPE

The need to accurately determine a spacecraft's position relative to its supporting ground station, other spacecraft, and its intended target is fundamental to space navigation. In its basic form, the range measurement begins with a known ranging signal modulated onto an uplink, retransmitted by the spacecraft, and then detected on the downlink. The round-trip light time associated with this cycle yields a measurement of the range.

In non-regenerative ranging techniques, such as tone ranging for example, the on-board transponder performs phase demodulation and re-modulation of the carrier only. When the ranging signal is turned around or retransmitted by the spacecraft, the uplink noise is also modulated onto the downlink carrier, incurring a path loss of $1/r^4$. For typical deep space missions, the noise power in the transponder ranging channel may be 30 to 40 dB greater than the ranging power, thereby degrading the ranging measurement precision.

The need for greater ranging accuracies is evident as new generations of interplanetary space missions are required to perform orbit insertions, gather radio science data, or travel to more distant planets, thereby incurring greater path losses. Regenerative ranging provides a method for removing the uplink noise contributions from the downlink signal, thereby increasing the Signal-to-Noise Ratio (SNR) at the ground station ($1/r^2$ vs. $1/r^4$), resulting in better range precision and the ability for the link designer to allocate more power to the telemetry.

The CCSDS has addressed this issue by providing recommendations for two cases of regenerative ranging, one where ranging accuracy is a priority, and the other where acquisition time is of primary concern. A recommendation for transparent (non-regenerative) ranging is also put forth. These recommendations were selected based on evaluating performance in several key metrics, including: range measurement accuracy, acquisition time, interference to telecommand/telemetry, and hardware implementation.

This Green Book is an adjunct document to the CCSDS Recommended Standard, *Pseudo-Noise (PN) Ranging Systems* (reference [1]).

1.2 APPLICABILITY

For the reasons outlined in the previous subsection, namely the substantial gains in SNR (up to 30 dB) at the ground station, the two regenerative ranging techniques put forth in reference [1] are particularly well suited for long-range deep space missions as well as Lagrangian missions, where a low signal-to-noise environment exists. These are the Tausworthe, ν=4 (T4B) ranging code, applicable to scenarios where ranging accuracy is a priority, and the Tausworthe, ν=2 (T2B), for range measurements where acquisition time is of primary concern. The latter code is also recommended for the transparent, or turnaround, ranging application, where high accuracy ranging is not required.

These codes are not intended for Code Division Multiple Access (CDMA) applications or for power flux density reductions, because of the strong spectral component at the range clock frequency.

In no event will CCSDS or its members be liable for any incidental, consequential, or indirect damages, including any lost profits, lost savings, or loss of data, or for any claim by another party related to errors or omissions in this report.

1.3 CONVENTIONS AND DEFINITIONS

1.3.1 DEFINITIONS

The following definitions apply throughout this Report:

chip rate: rate at which the PN code bits (or 'chips') are transmitted.

coherent transponder: transponder for which the downlink carrier is phase-coherent with the received uplink carrier.

component sequences: family of shorter-length PN sequences used to form the ranging PN code using logic operations.

range clock: PN component code with the highest frequency (i.e., shortest period); determines the range resolution.

regenerative ranging: type of ranging where the spacecraft demodulates and acquires the ranging code by correlation with a local code replica from the uplink ranging signal, and regenerates the ranging code on the downlink.

transparent ranging: type of ranging where the spacecraft frequency-translates the uplink ranging signal to the downlink without code acquisition (i.e., non-regenerative ranging or turnaround ranging).

one-way jitter: ranging jitter in meters resulting from measuring the round-trip light time and halving the measurement to compute the distance.

1.3.2 CONVENTIONS

In this document, the following convention is used:

– A '+1' ranging chip corresponds to a binary 0 value;

– A '-1' ranging chip corresponds to a binary 1 value.

1.3.3 ABBREVIATIONS AND ACRONYMS

B_L	one-sided loop noise bandwidth
c	speed of the light
C_i	components or probe sequence (i =1...6)
CTL	Chip Tracking Loop
DTTL	Data Transition Tracking Loop
E_c	Energy of the chip (W/Hz)
$2E_C /N_0$	chip signal-to-noise ratio (energy of the chip over single-sided noise spectral density)
F_c	chip rate (Hz)
f_{RC}	frequency of the ranging clock (Hz)
L	PN sequence length (number of chips)
L_i	length of the probe sequence C_i (number of chips)
N_0	one-side noise power spectral density (W/Hz)
NCO	Numerically Controlled Oscillator
P_{ACQ}	probability of acquisition (for the ranging sequence)
PN	Pseudo Noise
P_R	power of the ranging signal (Watt)
P_{RC}	power of the ranging clock component (Watt)
P_R/ N_0	ranging power over noise power spectral density (Hz)
r.v.	random variable
T_{ACQ}	ranging acquisition time (s)
$T_{ACQ\_S/C}$	spacecraft ranging acquisition time (s)
$T_{ACQ\_G/S}$	station ranging acquisition time (s)
TC	telecommand
T_c	chip period (s)
TM	telemetry
$T_r = LT_c$	one sequence length
T4B	weighted-voting balanced Tausworthe, voting ν=4
T2B	weighted-voting balanced Tausworthe, voting ν=2
ξ	in-phase fractional correlation
ψ	out-of-phase fractional correlation.
ρ^*_{ik}	normalized correlation coefficients (i.e., unit amplitude and correlation time equal to one sequence length $T_r = LT_c$)
λ	correlation scale factor

1.4 REFERENCES

The following documents are referenced in this Report. At the time of publication, the editions indicated were valid. All documents are subject to revision, and users of this Report are encouraged to investigate the possibility of applying the most recent editions of the documents indicated below. The CCSDS Secretariat maintains a register of currently valid CCSDS documents.

[1] *Pseudo-Noise (PN) Ranging Systems*. Recommendation for Space Data System Standards, CCSDS 414.1-B-1. Blue Book. Issue 1. Washington, D.C.: CCSDS, March 2009.

[2] J. L. Massey, G. Boscagli, and E. Vassallo. "Regenerative Pseudo-Noise (PN) Ranging Sequences for Deep-Space Missions." *International Journal of Satellite Communications and Networking* 25 , no. 3 (28 Feb 2007): 285-304.

[3] "Module 214, Pseudo-noise and Regenreative Ranging." In *DSN Telecommunications Link Design Handbook. Rev. E. DSN No. 810-005*. Pasadena California: JPL, January 15, 2001.

[4] R. C. Titsworth.[1] "Optimal Ranging Codes." *IEEE Transactions on Space Electronics and Telemetry* 10, no. 1 (March 1964): 19-30.

[5] G. Boscagli, et al. "PN Regenerative Ranging and Its Compatibility With Telecommand and Telemetry Signals." *Proceedings of the IEEE* 95, no. 11 (November 2007): 2224 - 2234.

[6] G. Boscagli, et al. "On Open and Closed Loop Ranging Jitter Performance (AI_07-07)." CCSDS Ranging Working Group.

[7] M. Visintin and M. Mondin. *Performance-Based Evaluation of Selected PN Ranging Codes for On-Board Regeneration*. ESOC Contract 18689/04/D/C (EuroConcepts).

[8] G. Boscagli, P. Holsters, and L. Simone. "Propose[d] Figures for XPND Linearity, Gain Flatness, 3 dB Bandwidth and Group Delay Variation for the Selected PN Ranging Scheme(s)." CCSDS Ranging Working Group, 9 November-2 December 2005.

[9] W. C. Lindsey and M. K. Simon. *Telecommunication Systems Engineering*. Englewood Cliffs, New Jersey: Prentice-Hall, 1973.

[10] G. Boscagli, E. Vassallo, and M. Visintin. "Reciprocal Influence between Ranging Codes and TC/TM." CCSDS Ranging Working Group, 29 November-2 December 2005.

[1] Subsequent to publication of this paper, the author changed his surname to Tausworthe.

[11] P. Holsters. "Complete the Transparent Channel Analysis by Including the TC Signal with a Low Pass Transponder Channel (AI_06-03)." CCSDS Ranging Working Group, October 2007.

[12] G. Boscagli and P. Holsters. "Influence of Transparent Ranging Channel on the Acquisition Time (AI_05-07)." CCSDS Ranging Working Group, 12-16 June 2006.

[13] M. Maffei, L. Simone, and G. Boscagli. "PN Ranging Acquisition Performance Results Based on Threshold Comparison with Soft and Hard Quantized Correlators." CCSDS Ranging Working Group, 26-30 October 2009.

[14] *Radio Frequency and Modulation Systems—Part 1: Earth Stations and Spacecraft*. Recommendation for Space Data System Standards, CCSDS 401.0-B-20. Blue Book. Issue 20. Washington, D.C.: CCSDS, April 2009.

[15] E. Vassallo and M. Visinti. "PN Ranging Signal Spectra." CCSDS Ranging Working Group, 26-30 October 2009.

2 PN REGENERATIVE RANGING SYSTEMS

2.1 FUNDAMENTALS OF PN RANGING SCHEMES

A *ranging-sequence system* is a system in which a periodic binary (±1) ranging sequence modulates an uplink carrier[2] to produce a signal that is transmitted from an Earth station to a transponder in the spacecraft whose range from the Earth station is to be measured. This modulated uplink carrier is received and processed by the spacecraft transponder, either in a simple turnaround (non-regenerative) manner or by detection and regeneration to remove uplink noise, and then retransmitted to the Earth station where the round-trip delay between the transmitted and received signals is measured. Regenerative ranging provides such a substantial power advantage over non-regenerative ranging, up to 30 dB in proposed systems that it can be expected to be the baseline in most of future deep space missions. The term 'Pseudo-Noise (PN) ranging' refers in a strict sense to the use of a ranging-sequence system in which the ranging sequence is a logical combination of the so-called range clock-sequence and several Pseudo-Noise (PN) sequences. The range clock sequence is the alternating +1 and –1 sequence of period 2. A Pseudo-Noise (PN) sequence is a binary ±1 sequence of period L whose periodic autocorrelation function has peak value $+L$ and all $(L-1)$ off-peak values equal to –1. Figure 2-1 illustrates a portion of such a ranging-sequence waveform and the corresponding range-clock waveform, which is just a square-wave of fundamental frequency $f_{RC} = \frac{1}{2T_C}$.

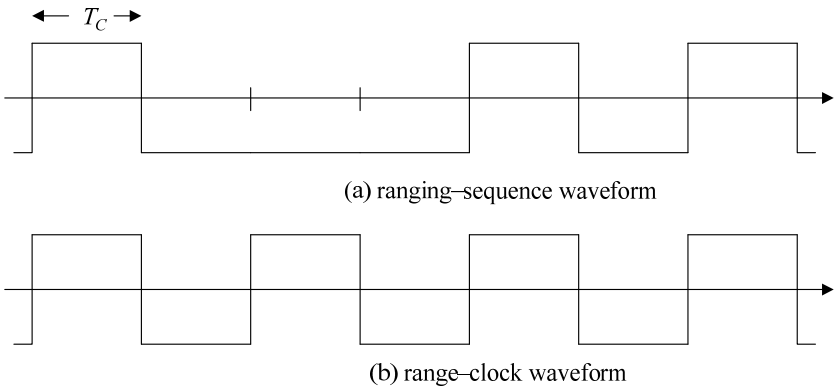

(a) The ranging-sequence waveform for the chip pattern ...+1 –1 –1 –1 +1 –1 +1...
(b) the corresponding range-clock waveform for a rectangular chip waveform.

Figure 2-1: Ranging-Sequence Waveform

In all practical ranging systems, the ranging sequence is acquired by the receiver as the result of correlations between the received sequence and certain ±1 periodic sequences (and their cyclic shifts), referred to as *probing sequences*, whose periods are divisors of the ranging-sequence period. The probing sequences are related in some manner to the ranging

[2] For standard telemetry and communications (TT&C), phase modulation is used.

sequence; e.g., the ranging sequence might be the sequence resulting from some sort of voting by the chips of all the probing sequences at the same chip time. A correlation (i.e., chip-by-chip multiplication followed by a summation) of the received ranging sequence is made with a model of each probing sequence and its distinct cyclic shifts to determine which cyclic shift is 'in-phase' with the received sequence over the portion of the received sequence where the correlation is performed. The probing sequences must have the property that, when all these 'in-phase' decisions are correctly made, they determine the delay (modulo the ranging sequence period *L*) in chips of the received ranging sequence relative to its corresponding model (local replica).

There are two *important quality measures* for probing sequences:

– acquisition time;

– spectral properties.

Acquisition time refers to the time required to carry out the correlations for the probing sequences and their cyclic shifts and should be as small as possible. Because it is the presence in the ranging sequence of a component proportional to a probing sequence that determines the effectiveness of correlating with that probing sequence, the spectra of the probing-sequence waveforms should be such that they are not substantially attenuated by the filtering at the transmitter of the ranging sequence as may be required to avoid interference between the ranging signal and other TT&C signal components (e.g., telemetry signals).

The two *important quality parameters* of the ranging measurement are

– its random-noise variation;

– its ambiguity resolution.

The first task of the receiver (after the phase demodulation of the received phase-modulated signal) is to lock onto the range clock. The clock tracking jitter (due to thermal noise) determines the standard deviation of the measurement error in meters.

After locking onto the range clock, the receiver correlates in some manner a model of the ranging sequence with the received ranging sequence to determine the integer number of chips, modulo the period *L* in chips of the ranging sequence, that the signal has been delayed in its round trip from the Earth station. The (one-way) ambiguity due to the period of the ranging sequence in meters is

$$U = \frac{1}{2} c \cdot L \cdot T_c = \frac{c \cdot L}{4 f_{RC}}$$

For example, with L = 1,009,470 chips and $f_{RC} = 10^6$ Hz, $U \approx$ 75,710,000 m or about 75,710 km.

In the analysis for the evaluation of the acquisition time for the different ranging sequences, one of the main reference parameters is the chip SNR $2E_C / N_0$ where E_C is the received chip

energy and $N_0/2$ is the two-sided noise power spectral density of the additive Gaussian noise. This can be related to the ranging signal-to-noise spectral density ratio as

$$\frac{2E_C}{N_0} = \frac{1}{f_{RC}} \cdot \frac{P_R}{N_0}$$

It is worth pointing out that a range-clock frequency of $f_{RC} = 10^6$ Hz and P_R/N_0 of +27 dBHz gives a signal-to-noise spectral density ratio $2E_C / N_0$ of –33 dB.

2.2 PN CODE STRUCTURE

2.2.1 GENERAL

There are two PN codes recommended for regenerative ranging by the PN ranging standard. Both codes have similar structure and come from the same family of PN codes, but differ in the strength of the ranging clock component.

The first PN code is called the weighted-voting (ν=4) balanced Tausworthe code, and is abbreviated as T4B. This code has a stronger ranging clock component, and will provide greater ranging accuracy at the expense of slightly longer acquisition time. Thus the T4B code should be used for ranging systems where ranging accuracy is of primary concern, such as for radio science.

The other recommended PN code is the weighted-voting (ν=2) balanced Tausworthe code, abbreviated as T2B. This code has a weaker ranging clock component relative to the other components and will have a faster acquisition time at the expense of greater jitter in the ranging measurements. The T2B code should be used for ranging systems where acquisition time is of primary concern, for example, in missions where the expected ranging SNR is very low.

2.2.2 T4B PN CODE GENERATION

The structure of both the T4B and T2B codes is based on a composite code built from logical combinations of six periodic component PN sequences, originally derived by Tausworthe (reference [4]). The six component sequences are shown in table 2-1.

Table 2-1: Component PN Sequences

Code	Component Length	Chip Sequence
C_1	2	1, -1
C_2	7	1, 1, 1, -1, -1, 1, -1
C_3	11	1, 1, 1, -1, -1, -1, 1, -1, 1, 1, -1
C_4	15	1, 1, 1, 1, -1, -1, -1, 1, -1, -1, 1, 1, -1, 1 -1
C_5	19	1, 1, 1, 1,-1, 1, -1, 1, -1, -1, -1, -1, 1, 1, -1, 1, 1, -1, -1
C_6	23	1, 1, 1, 1, 1, -1, 1, -1, 1, 1, -1, -1, 1, 1, -1, -1, 1, -1, 1, -1, -1, -1, -1

Each component sequence is placed in a circular shift register with length equal to the component length and clocked at the chip rate. The T4B composite code is formed from the combination of the shift register outputs using the following formula:

$$C = sign(4C_1 + C_2 - C_3 - C_4 + C_5 - C_6)$$

The output of each shift register is fed back to the input, such that each component repeats itself with period equal to the component length. Figure 2-2 shows a functional block diagram of the T4B PN code generation.

Because of the *sign* function, the value of the composite code C in the formula above can be interpreted as being determined by votes from the six component sequences (the negative sign simply means that the component sequence is inverted). C_1 is multiplied by four, and thus has four 'votes', while the other five components only have one vote. Since the C_1 component is the range clock component, the T4B code has a relatively strong clock component.

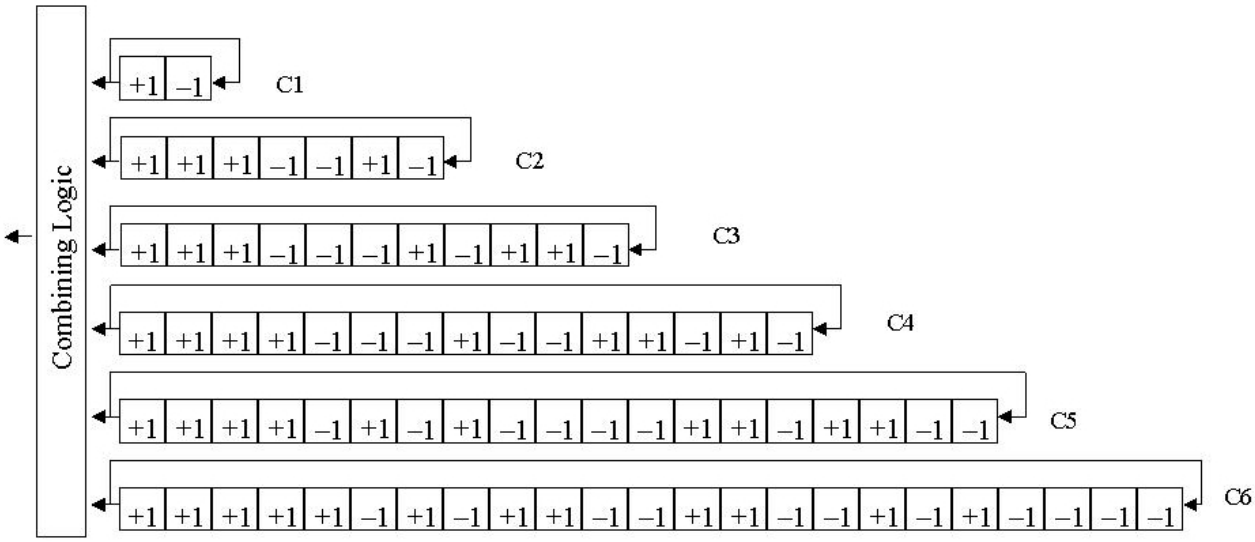

where the combined sequence is $C = sign(4C_1 + C_2 - C_3 - C_4 + C_5 - C_6)$

Figure 2-2: T4B PN Code Generation

2.2.3 T2B PN CODE GENERATION

The component sequences used for the T2B code are identical to those used for T4B. The combination logic to form the T2B composite code is given by:

$$C = sign(2C_1 + C_2 - C_3 - C_4 + C_5 - C_6)$$

The combination logic is identical to that used to generate the T4B code, except the C_1 component is weighted only by a factor of two (i.e., two votes). Thus this code has a weaker range clock component. Figure 2-3 shows a block diagram of the T2B PN code generation.

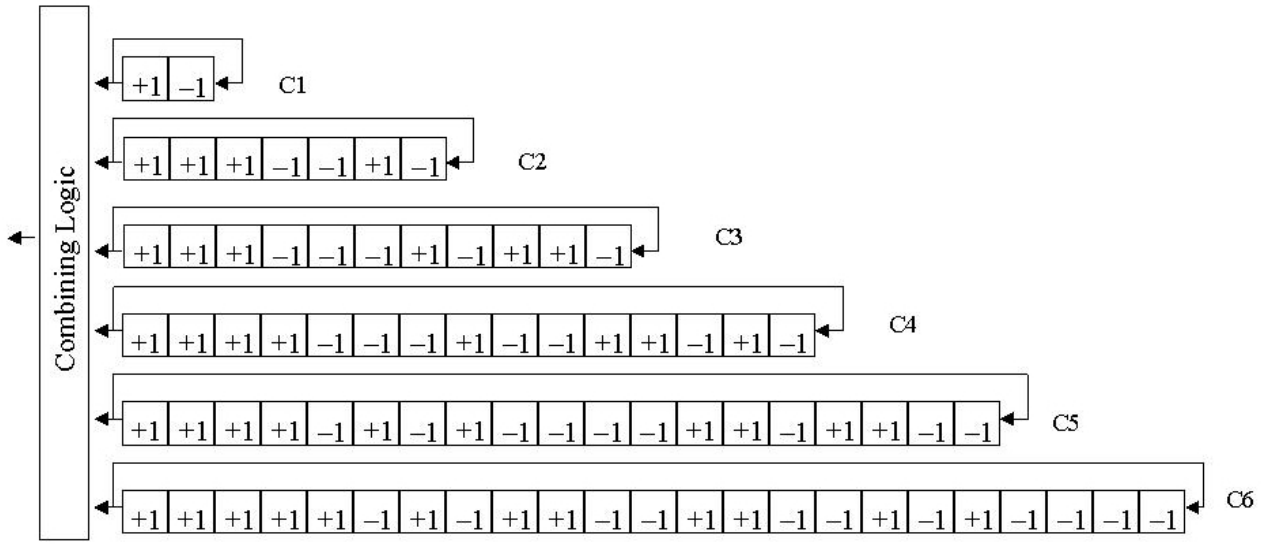

where the combined sequence is $C = sign(2C_1 + C_2 - C_3 - C_4 + C_5 - C_6)$

Figure 2-3: T2B PN Code Generation

2.2.4 CODE PROPERTIES

2.2.4.1 Code Length

The lengths of the component sequences for T4B and T2B are all relatively prime, so the composite code will have a period equal to the product of the component lengths. Since the component sequences are identical for both codes, the composite code length L for the T4B and T2B codes is:

$$L = 2 \times 7 \times 11 \times 15 \times 19 \times 23 = 1{,}009{,}470 \; chips$$

2.2.4.2 Code Imbalance

Another code property of interest is the balance between the number of 1s and -1s in the composite sequence. An imbalance will result in a DC component in the PN code spectrum. It is best to minimize the code imbalance, since energy in the DC component cannot be used for ranging. By inverting components C_3, C_4, and C_6 (as done in the combining logic), the code imbalance can be reduced. Table 2-2 shows the code imbalance for the T4B and T2B codes.

Table 2-2: Code Imbalance

	Sequence Length	Number of 1s	Number of -1s	Longest run of 1s	Longest run of -1s	Imbalance	DC Value
T4B	1009470	504583	504887	7	5	304	3.01E-4
T2B	1009470	504033	505437	9	9	1404	1.39E-3

2.2.4.3 Range Clock Attenuation

The range clock attenuation is a measure of the strength of the range clock in the composite sequence relative to an unmodulated squarewave (i.e., an alternating 1, -1) pattern. This has a direct effect on the ranging accuracy. The range clock attenuation is inversely related to the number of transitions in the composite sequence, as shown in table 2-3.

Table 2-3: Range Clock Attenuation

	Number of Transitions	Range Clock Attenuation
T4B	945480	0.550 dB
T2B	717618	4.049 dB

2.2.4.4 Correlation Properties

The correlation between the composite PN code and the component sequences is also important. There are two correlation values to be considered. The in-phase correlation occurs when the component sequence is aligned with its respective component in the composite PN code. The out-of-phase correlation occurs when the component sequence is delayed by 1 to L-1 chips (where L is the length of the component sequence) relative to its respective component in the composite PN code. For the clock component, the out-of-phase correlation is always the negative of the in-phase correlation (antipodal signal).

Table 2-4 shows the in-phase and out-of-phase correlation values for the T4B and T2B PN codes. The correlations are computed over the entire length of the composite PN code by repeating each component sequence until the lengths are identical. The normalized in-phase and out-of-phase correlation values can be used to compute the acquisition time of the ambiguity-resolving components (e.g., C_2 through C_6). The normalized in-phase correlation of C_1 determines the range clock attenuation as:

Range Clock Attenuation = – 20 log (C_1 in-phase correlation/sequence length)

Table 2-4: In-Phase and Out-of-Phase Correlation

	T4B In-phase Correlation	T4B Out-of-phase correlation	T2B In-phase Correlation	T2B Out-of-phase correlation
C_1	947566	-947566	633306	-633306
C_2	61904	-10368	247020	-41404
C_3 (inverted)	61904	-6160	250404	-24900
C_4 (inverted)	61904	-4400	251332	-17852
C_5	61904	-3456	251604	-14056
C_6 (inverted)	61904	-2800	251940	-11388

2.2.5 SPECTRAL PLOTS

The measured spectra for the two recommended Tausworthe schemes (T4B and T2B) with square-wave shaping (see 2.3) are presented in the following figures (see figures 2-4, 2-5, 2-6, and 2-7) for various frequency spans and applying the following modulation parameters:

– Chip rate = 2.5 Mchip/s;

– Carrier frequency at 10 MHz;

– Modulation index = 1 rad-pk.

In general:

– strong clock component at one half of the chip rate or at the clock frequency (1.25 MHz);

– sin(x)/x shape, due to effect of the longer repetition components that determine the pseudo-randomness of the code, with nulls at multiples of the chip rate;

– discrete component at odd multiples of the clock frequency;

– different power distribution for the PN code components for the different codes (due to different majority voting weight).

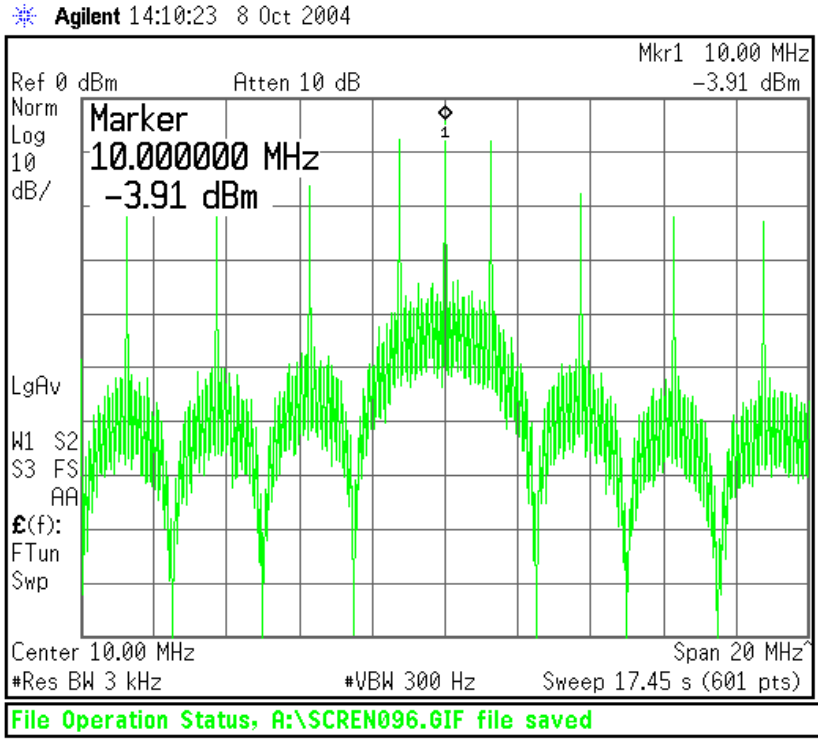

Figure 2-4: T4B Spectrum

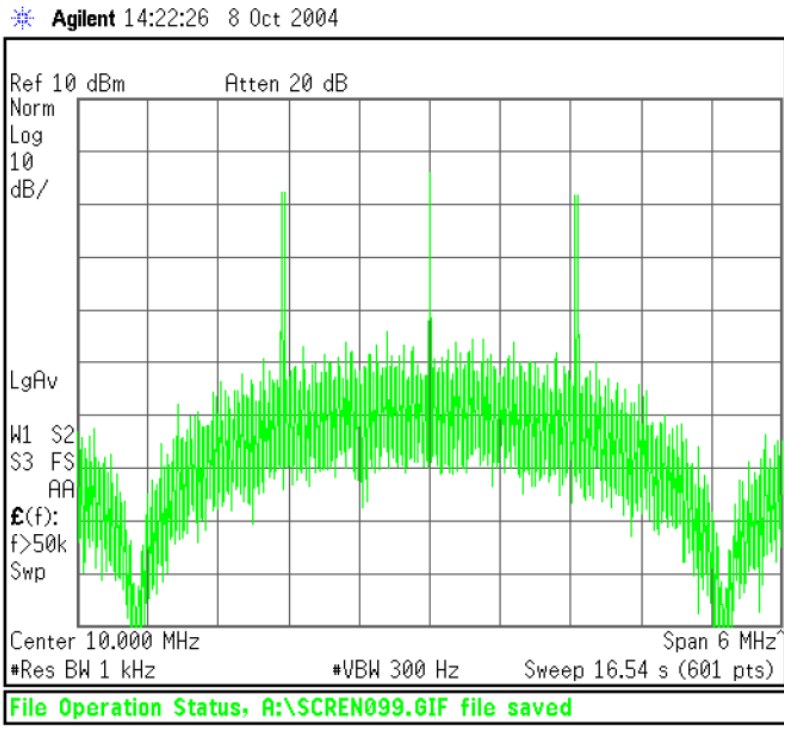

Figure 2-5: T4B Spectrum Close-Up

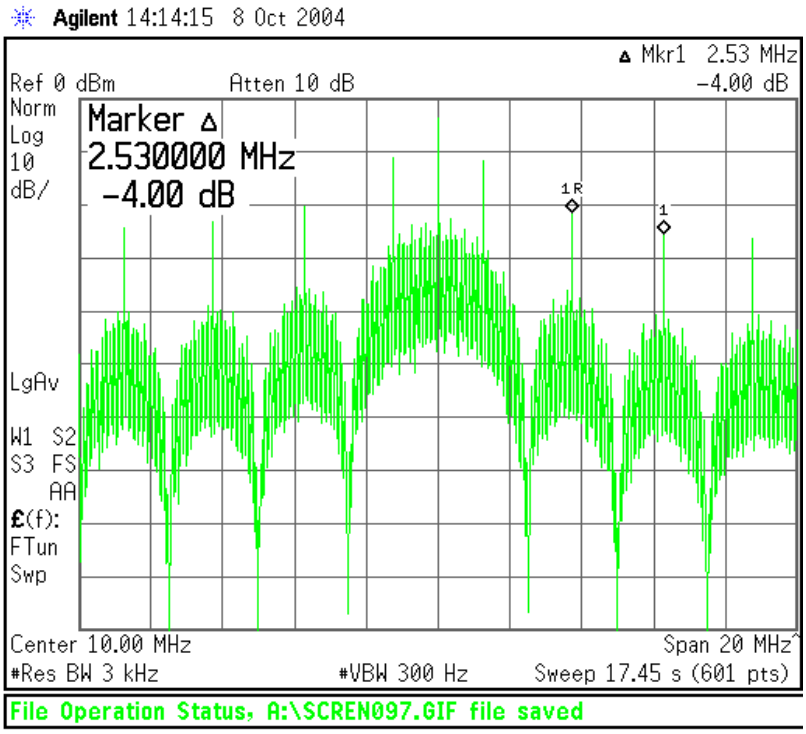

Figure 2-6: T2B Spectrum

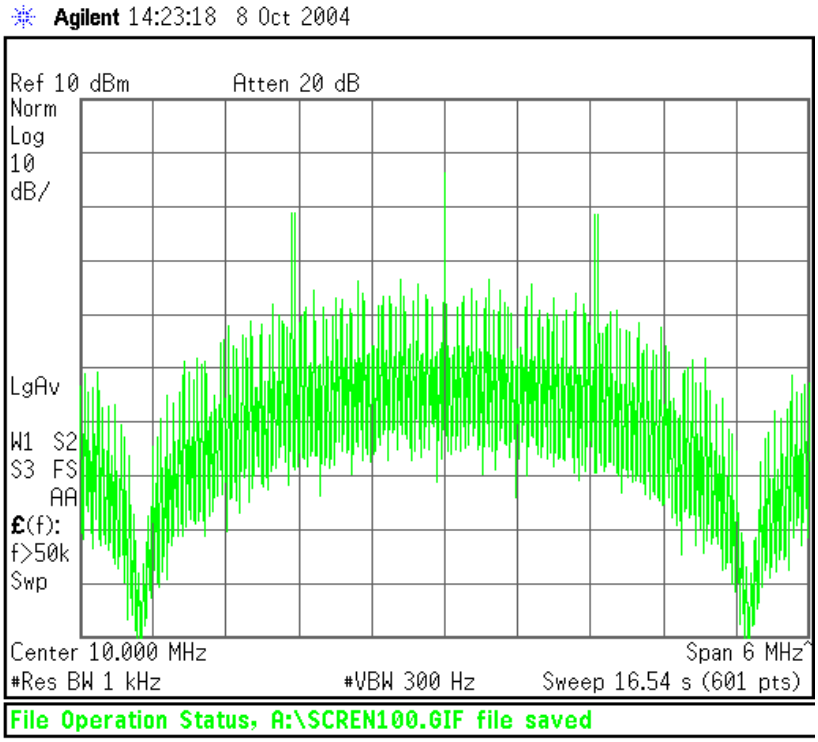

Figure 2-7: T2B Spectrum Close-Up

Similar plots have been obtained by measurements for the sine-wave shaped case (see 2.3) as given in figures 2-8 and 2-9:

– Chip rate = 1 Mchip/s;

– Carrier frequency at approx 9.56 MHz;

– Modulation index = 0.75 rad-pk.

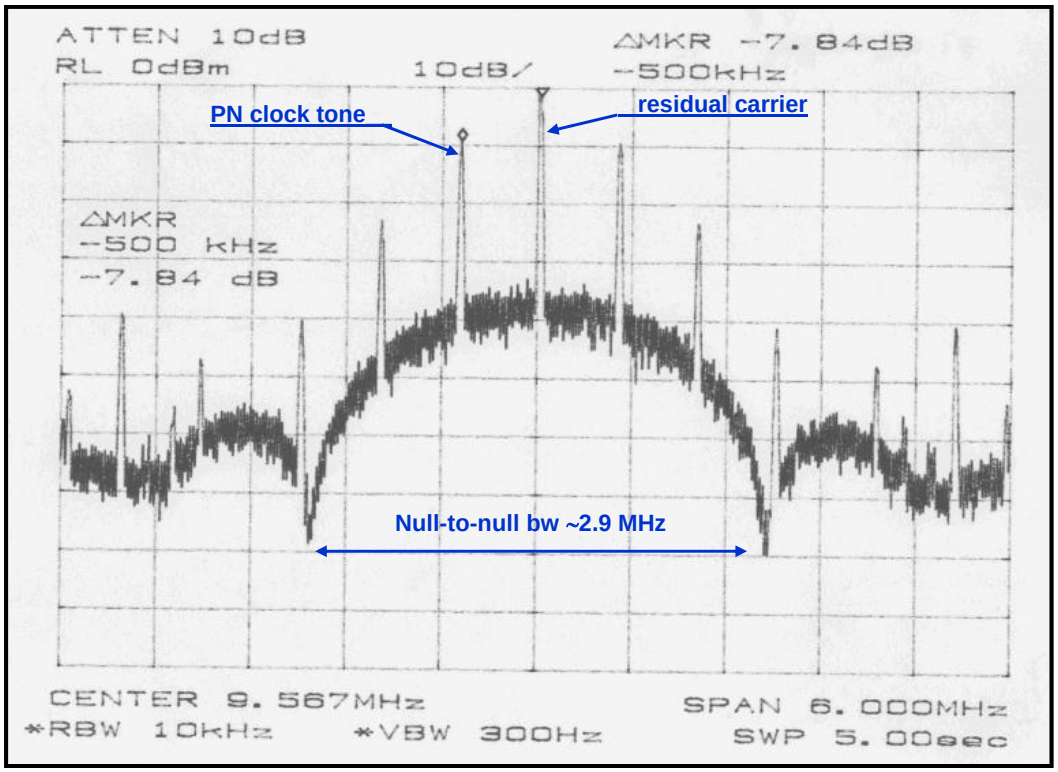

Figure 2-8: T4B

Theoretical derivations explaining the given measured spectral plots and additional theoretical and simulated spectral plots can be found in references [7] and [15]. The conclusions on the spectral properties for this case are:

– strong clock component at one half of the chip rate or at the clock frequency (0.5 MHz);

– continuous spectrum with nulls (except the first) at odd (n>3) multiples of the clock frequency and faster decay relative to squarewave shaping;

– first null position function of the modulation index and equal to three times the clock frequency (1.5 MHz) only when the modulation index is small;

– discrete component at integer even and odd multiples of the clock frequency;

– different power distribution for the PN code components for the different codes (due to different majority voting weight).

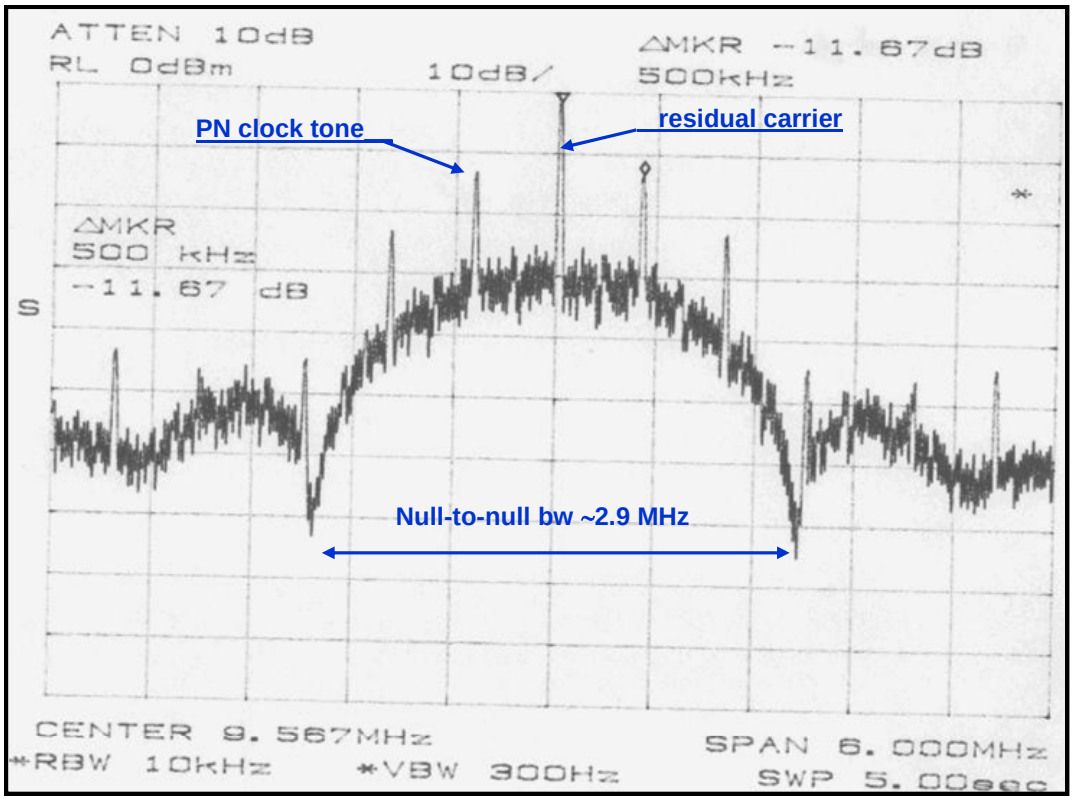

Figure 2-9: T2B

2.3 MODULATION

2.3.1 GENERAL

The PN ranging code is linearly phase modulated on the uplink and downlink carrier; i.e., a positive transition of -1 to +1 in the baseband code results in an advance of the transmitted RF carrier phase.

Normally, the PN ranging signal has a squarewave shape. However, baseband shaping may be required by mission design to conserve bandwidth at high chip rates. In this case the shaping filter has the following impulse response (sinewave shaping):

$$h(t) = h_{\sin}(t) = \begin{cases} \sin(\pi t / T_c) & t \in [0, T_c] \\ 0 & elsewhere \end{cases}$$

where T_c is the chip duration.

The selected modulation scheme is such that ranging, telemetry, and telecommand as specified in CCSDS 401.0-B (2.2.4) and (2.2.7) (reference [14]) can be performed at the same time.

The effect of squarewave and sinewave shaping on the actual transmitted spectrum can be seen in 2.2.5.

2.3.2 UPLINK CHIP RATE

The PN Ranging Blue Book (reference [1]) specifies the possible chip rates to be used and the coherency with the carrier frequency. The purpose of having the code rate coherent with the uplink carrier is to ease the code acquisition by pre-steering the code PLL with the carrier frequency.

The Blue Book also specifies that:

> The configuration of some CCSDS Agencies' ground stations may not be able to easily implement the above ratios between chip rate and carrier frequency. In such cases, the offset between the generated value and the theoretical value shall be < 10 mHz. However, the chip rate shall remain locked to the station frequency reference.

It is now quite common to generate a chip sequence by using an NCO. The frequency output of the NCO is given by the input frequency of a master clock divided by 2^N multiplied by an integer value of n, where N is the number of bits of the NCO.

As an example, if the master oscillator is at 17.5 MHz and N=32, it will have a frequency resolution of 17.5 MHz/ 2^{32} = 4.07 mHz.

The code acquisition and tracking loop will have to accurately regenerate the code clock phase using the received carrier frequency for pre-steering the code clock Phase Locked Loop (PLL).

The Blue Book also specifies a minimum P_R/N_0 of 10 dBHz for the ranging signal in the Earth-to-space link. The selection of the PLL loop bandwidth and loop order must therefore take into account the possible frequency offset up to 10 mHz.

The phase of the carrier and the group delay of the ranging code are affected in the opposite direction when the signal is going through a varying ionospheric layer or charged plasma. These effects should be continuously tracked in the on-board processing.

Missions operating with a low signal to noise spectral density at or near -10 dBHz at the receiving ground station will require a very narrow clock PLL bandwidth. In this case the Doppler pre-steering compensation in the receiving ground station needs to consider the actual uplink code rate. This is particularly important when the code generation is done with NCOs resulting in a numerical rounding error.

2.4 ON-BOARD ACQUISITION

2.4.1 INTRODUCTION

The theoretical on-board acquisition time (from the Blue Book) and the analysis reported in this subsection are based on ideal linear channel and an on-board processing implementing:

a) six parallel correlators;

b) maximum search algorithm;

NOTE – It is shown in the following that the maximum search corresponds to the optimum receiver solution.

c) perfect carrier demodulation (the carrier tracking loop jitter degradation is not considered);

d) perfect chip tracking (the CTL jitter degradation is not considered);

e) no impacts due to amplitude quantization of the signal at the output of the chip detection filter (matched filter);

f) no impacts due to time quantization (number of samples per chip).

In addition the degradation due to uplink telecommand interference (although negligible) is not considered in this analysis; it is analyzed in 2.8.

2.4.2 ON-BOARD DSP ARCHITECTURE FOR REGENERATIVE CHANNEL

The on-board regenerative ranging operations are accomplished in two stages: the received ranging clock component is first acquired, and, once this has taken place, the ranging code position is searched, acquired, and tracked. Figure 2-10 shows the regenerative ranging channel as currently implemented in the BepiColombo pre-development model of the X/X/Ka deep space transponder. It includes the following functions:

a) CTL for phase and frequency recovery of the code chip and proper generation of the synchronization signal for the matched filter;

b) in-phase Integrator (matched filter);

c) one-bit quantization at matched filter output;

NOTE – The possibility to implement three-bit soft quantization (vs. ASIC complexity) is under investigation.

d) six correlators (one for each code component: C_1, C_2,…C_6) running in parallel for ranging code sequences position recovery;

e) downlink code generator function;

f) control logic for correlators and code generator management.

Each correlator implements a serial search over the L_i possible code phases of the related probe sequence C_i. For an optimum receiver, the L_i results are memorized for final comparison based on maximum search strategy; indeed the maximum value defines the correlation peak and the phase position of the probe sequence C_i inside the received ranging sequence. Simplified implementations consider the simpler threshold comparison approach, which seems more robust in terms of operating conditions, in particular in case of ranging channel active but no ranging signal present.

When the phases of all the 6 C_i components have been recovered, the position of the received ranging sequence is detected and the transmission of the ranging signal from the transponder can be enabled. In this way the downlink carrier is phase modulated by the reconstructed sequence, which is synchronized (same chip rate and same phase) with the received one.

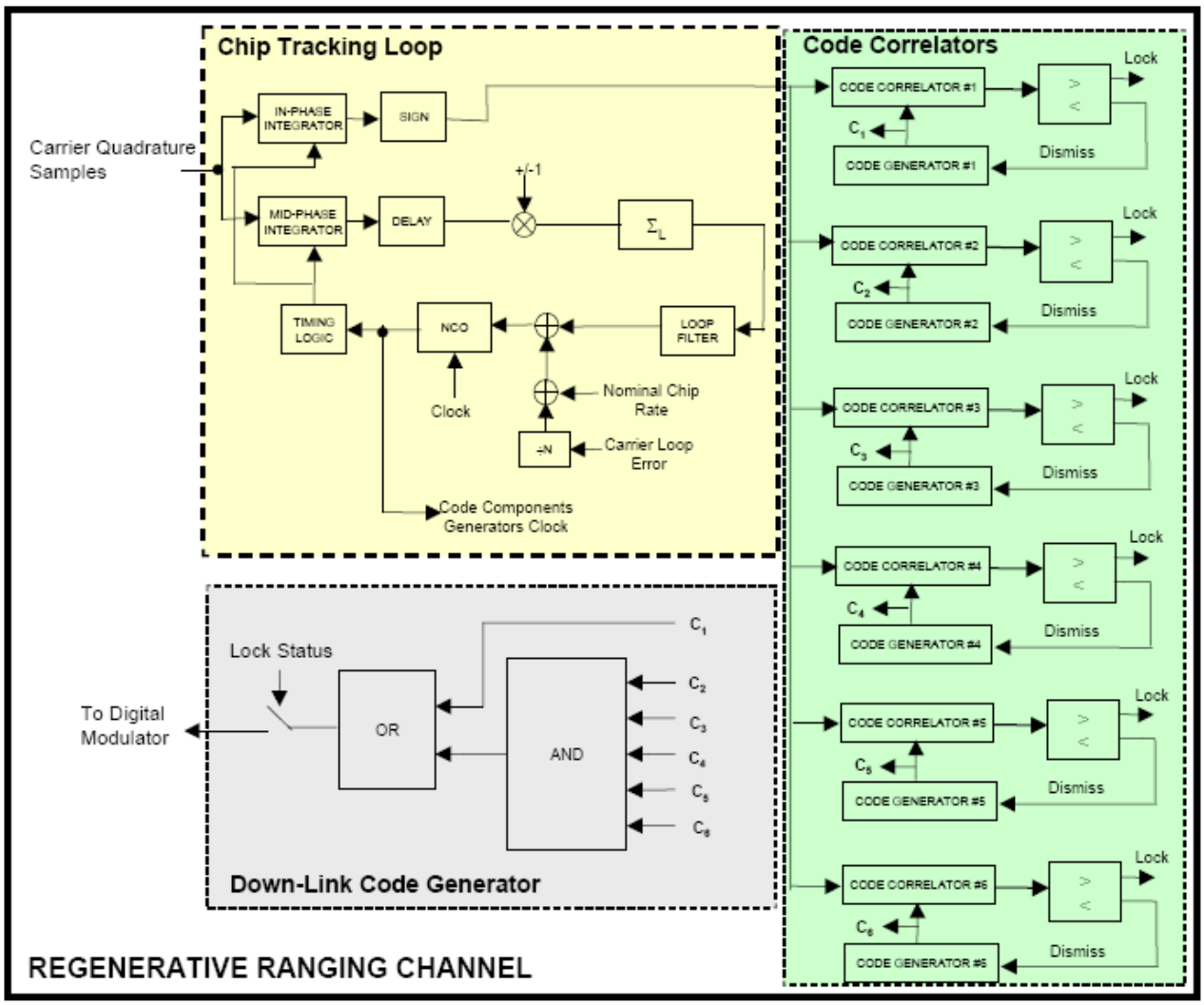

Figure 2-10: BepiColombo On-Board PN Regenerative Processing

2.4.3 PERFORMANCE EVALUATION

2.4.3.1 Simplified Analysis

2.4.3.1.1 General

In the analysis for the evaluation of the acquisition time for the different ranging sequences, one of the main reference parameters is the chip SNR $2E_C / N_0$, where E_C is the received chip energy and $N_0 / 2$ is the two-sided noise power spectral density of the additive Gaussian noise. This can be related (see 2.4.3.1.2) to the ranging signal-to-noise spectral density ratio as

$$\frac{2E_C}{N_0} = \frac{1}{f_{RC}} \cdot \frac{P_R}{N_0}$$

Next is set up a metric that facilitates comparison of the acquisition time for various ranging-sequence schemes. As the standard for comparison, a decision between antipodal alternatives, such as the decision between the range clock sequence C_1 and its right cyclic shift, is chosen. In this case the probability of error P_{e2} for an in-phase decision, assuming an integration time of K chips with energy E_C per chip and unity in-phase fractional correlation when the noise is additive white Gaussian with two-sided power spectral density $N_0/2$, is given by:

$$P_{e2} = Q\left(\sqrt{2KE_c / N_0}\right)$$

where

$$Q(x) = \frac{1}{\sqrt{2\pi}} \int_x^\infty e^{-t^2/2} dt$$

P_{e2} can also be written in terms of the Euclidean distance d and rms noise value σ:

$$P_{e2} = Q\left(d / 2\sigma\right)$$

where, using the normalization of 2.4.3.1.2.

$$d = 2K$$

$$\sigma = \sqrt{(KN_0)/(2E_c)}$$

Equivalently, the number K_a of chips needed for a given P_{e2} with antipodal sequences having unity in-phase fractional correlation is $K_a = \dfrac{\left[Q^{-1}(P_{e2})\right]^2}{2E_c/N_0}$.

The number K_a of chips needed for a given P_{e2} with antipodal sequences having unity in-phase fractional correlation is very mildly dependent on the value of P_{e2} for any specified value of the chip SNR, as demonstrated in reference [2].

Applying the considerations reported in 2.4.3.1.3, it is shown that $P_{e2} \approx 5\times10^{-5}$ corresponds to a probability of successful acquisition of the ranging sequence of about 0.999 (99.9%) and K_a is about 30000 chips for $2E_C/N_0$ = -33 dB; this is the approximate figure uses in the examples in the following subsections.

For an arbitrary probing sequence, the error probability P_{e2} in the decision between the in-phase cyclic shift and one of its out-of-phase cyclic shifts is a function of the in-phase fractional correlation ξ and out-of-phase fractional correlation ψ. The signal-space representation for this situation is shown in figure 2-11. The in-phase cyclic shift and the out-of-phase cyclic shift of the probing sequence correspond to the points C and E, respectively, on the circle of radius $K\xi$ (K being the number of correlated chips).

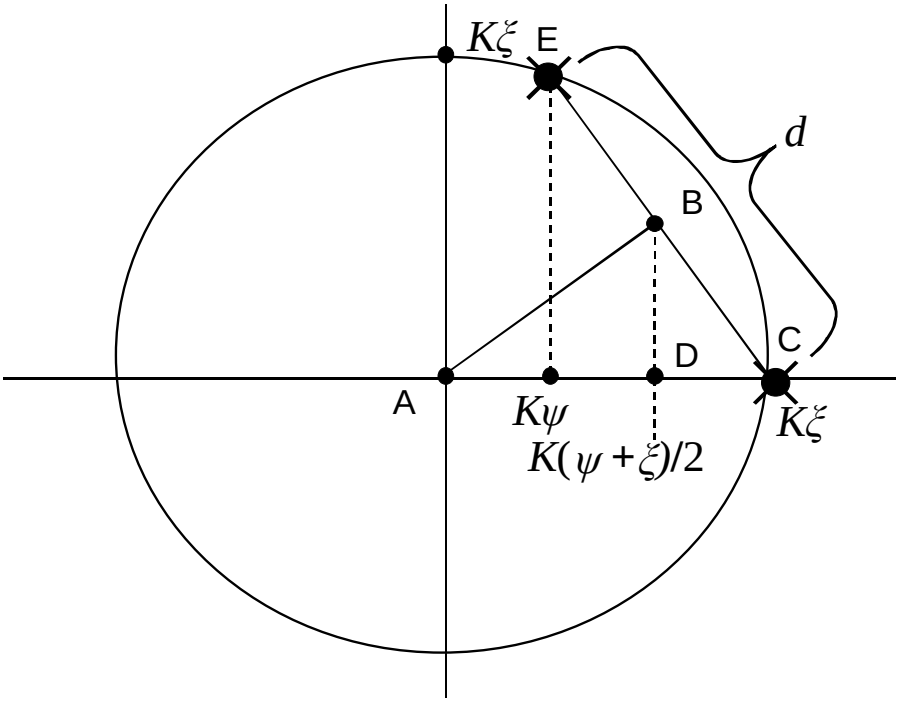

Figure 2-11: Signal-Space Representation for the Decision between the In-Phase Cyclic Shift and One of Its Out-of-Phase Cyclic Shifts of an Arbitrary Probing Sequence of Length *K* Chips, Having In-Phase Fractional Correlation ξ and Out-of-Phase Fractional Correlation ψ

Applying simple geometrical considerations to the similar triangles ABC and BCD, the squared Euclidean distance d^2 between the signals at points C and E is:

$$d^2 = 4 \cdot K^2 \cdot \xi^2 \cdot \lambda \quad \text{with} \quad \lambda = \frac{\xi - \psi}{2\xi}.$$

The parameter λ is the correlation scale factor for the probing sequence. For a decision between antipodal sequences, $\psi = -\xi$ so that $\lambda = 1$. For a decision between orthogonal sequences, $\psi = 0$ so that $\lambda = 1/2$.

Using the above expressions and following the approach used above for antipodal signals, it is shown that the number K of chips needed for a given P_{e2} and for any specified value of the chip SNR is

$$K = \frac{\left[Q^{-1}(P_{e2})\right]^2}{2E_c/N_0} \frac{1}{\lambda \cdot \xi^2}$$

This motivates defining the normalized correlation time (τ_{cor}) of an arbitrary probing sequence with parameters ξ and ψ as the ratio between K for the arbitrary probing sequence and K_a for antipodal sequence with unity in-phase fractional correlation as

$$\tau_{cor} = K / K_a = 1/(\xi^2 \cdot \lambda)$$

Finally assuming an acquisition strategy based on the maximum search and a single correlator for each probing sequence, it is possible to define the normalized acquisition time $\tau_{acq\text{-}Li}$ of the probing sequence C_i as

$$\tau_{\text{acq-Li}} = L_i \, \tau_{\text{cor}}$$

where L_i is the length of the probing sequence or, equivalently, the number of distinct cyclic shifts of that sequence. To find the normalized total acquisition time $\tau_{acq\text{-}tot}$, i.e., the normalized time required to acquire the phase of the entire ranging sequence, it can be assumed that all six probing sequences in the ranging-sequence scheme are correlated in parallel during the acquisition process, which requires six correlators. In this case $\tau_{acq\text{-}tot}$ is just the maximum of the normalized acquisition times $\tau_{acq\text{-}Li}$ of the six probing sequences, namely that of C_6, so that

$$\tau_{\text{acq-tot}} = \tau_{\text{acq-23}}$$

To convert the normalized time values (τ_{cor}, $\tau_{acq\text{-}Li}$, and $\tau_{acq\text{-}tot}$) to time measured in chips of the probing sequence, it is necessary only to multiply by the number of chips K_a needed to obtain the desired P_{e2} at the specified chip SNR for antipodal sequences with unity in-phase fractional correlation.

Table 2-5 (for v=2 balanced weighted-voting Tausworthe PN ranging-sequence) and table 2-6 (for v=4 balanced weighted-voting Tausworthe PN ranging-sequence) give the normalized correlation time τ_{cor}, together with the correlation time in chips (equal to 30000 τ_{cor}) required to achieve a pairwise error probability $P_{e2} = 5\times10^{-5}$ at a chip SNR $2E_C/N_0$ of –33 dB.

Table 2-5: v=2 Balanced Weighted-Voting Tausworthe PN Ranging-Sequence

Probing Sequence	ξ	ψ	λ	τ_{cor}	Correlation Time (Chips)
C_1 (range clock)	0.6274	–0.6274	1	2.54	76 200
C_2	0.2447	–0.0410	0.5838	28.61	858 300
-C_3	0.2481	–0.0247	0.5498	29.55	886 500
-C_4	0.2490	–0.0177	0.5355	30.12	903 600
C_5	0.2492	–0.0139	0.5279	30.50	915 000
-C_6	0.2496	–0.0113	0.5226	30.71	921 300
In-phase fractional correlation ξ, out-of-phase fractional correlation ψ, correlation scale factor λ and normalized correlation time τ_{cor}, together with the correlation time in chips required to achieve a pairwise error probability $P_{e2} = 5\times10^{-5}$ at a chip SNR $2E_C/N_0$ of –33.					

Table 2-6: v=4 Balanced Weighted-Voting Tausworthe PN Ranging-Sequence

Probing Sequence	ξ	ψ	λ	τ_{cor}	Correlation Time (Chips)
C_1 (range clock)	0.9387	–0.9387	1	1.13	33 900
C_2	0.0613	–0.0103	0.5840	455.7	13 671 000
-C_3	0.0613	–0.0061	0.5498	484.0	14 520 000
-C_4	0.0613	–0.0044	0.5359	496.6	14 898 000
C_5	0.0613	–0.0034	0.5277	504.3	15 129 000
-C_6	0.0613	–0.0028	0.5228	509.0	15 270 000
In-phase fractional correlation ξ, out-of-phase fractional correlation ψ, correlation scale factor λ and normalized correlation time τ_{cor}, together with the correlation time in chips required to achieve a pairwise error probability $P_{e2} = 5\times10^{-5}$ at a chip SNR $2E_C/N_0$ of –33 dB.					

Applying the previous equations reveals the total acquisition time in chips to be as in table 2-7. The table indicates also the acquisition time in seconds assuming a chip rate of 2 Mc/s (range clock frequency f_{RC} of 1 MHz and chip duration T_C as 0.5 μs)

Table 2-7: Normalized Acquisition Time ($\tau_{acq\text{-}tot}$) and Acquisition Time (T_{acq}) in Chips and Seconds Assuming f_{RC}=1 MHz and for the Error Probability $P_{e2} = 5\times10^{-5}$ and a Chip Signal-to-Noise Ratio $2E_C/N_0$ of -33 dB

Sequence	$\tau_{acq\text{-}tot} = \tau_{acq\text{-}23} = 23 \times \tau_{cor}$	T_{acq} (in chips)	T_{acq} (s)
T2B	23 × 30.71 = **706.3**	30,000 × 706.3 = **21,189,900**	**10.59**
T4B	23 × 509.0 = **11,707**	30,000 × 11,707 = **351,210,000**	**175.6**

It is interesting to observe that for the on-board acquistion time ($T_{ACQ\_S/C} = T_{ACQ}$ Spacecraft) the following general expression applies:

$$T_{ACQ\_S/C} = K_a \cdot \tau_{acq\_tot} \cdot \frac{1}{F_C} = \frac{\left[Q^{-1}(P_{e2})\right]^2}{2E_c/N_0} \tau_{acq\_23} \frac{1}{F_C} =$$

$$= \frac{\left[Q^{-1}(P_{e2})\right]^2}{2\dfrac{P_r}{N_0}\dfrac{1}{F_C}} 23 \cdot \tau_{corr} \frac{1}{F_C} \qquad = \frac{\left[Q^{-1}(P_{e2})\right]^2}{2\dfrac{P_r}{N_0}} 23 \cdot \frac{1}{\lambda \xi^2} =$$

$$= \frac{\left[Q^{-1}(P_{e2})\right]^2}{2\dfrac{P_r}{N_0}} 23 \cdot \frac{1}{\xi\left(\dfrac{\xi - \psi}{2}\right)}$$

where τ_{corr}, λ and ξ are related to C_6 (L_6 = 23).

It can be seen that:

– If the acquisition time is given as a function of the Ranging Signal Power over Noise Spectral Density (P_R/N_0 in dBHz), then the dependence on the chip rate disappears.

– If P_R/N_0 is reduced by 3 dB (i.e., from 27 to 24 dBHz), the acquisition time increases by a factor of 2, if P_R/N_0 is increased by 10 dB (i.e., from 27 to 37 dBHz), the acquisition is 10 times smaller. So the values in table 2-7 (evaluated for 27 dBHz) become respectively 5.29 s (for T2B) and 87.8 s (for T4B) for P_R/N_0 = 30 dBHz. Also the variation of the acqusition time based on the exponential law $10^{(Pr/No\text{-}30)/10}$ is demonstrated.

2.4.3.1.2 Normalization and Signal-to-Noise Ratio Definitions

The output of the phase-demodulator for the received ranging-sequence signal can be written as:

$$\sqrt{P_R}\,s(t) + n(t)$$

where

$$s(t) = s_k \text{ for } (k-1)T_C < t \le kT_C$$

is the binary (±1) ranging-sequence waveform with chip values $s_k \in \{+1, -1\}$, T_C is the chip duration, P_R is the power in the received ranging waveform, and $n(t)$ is white Gaussian noise with zero mean and autocorrelation function

$$R(\tau) = \frac{N_0}{2}\delta(\tau)$$

The output at time $t = kT_C$ of the matched filter for the rectangular chip waveform is

$$\frac{1}{T_C}\int_{(k-1)T_C}^{kT_C}\left[\sqrt{P_R}\,s(t) + n(t)\right]\,dt = \sqrt{P_R}\,s_k + \frac{1}{T_C}\int_{(k-1)T_C}^{kT_C} n(t)dt$$

Dividing by $\sqrt{P_R}$ yields the conveniently normalized matched-filter output

$$r_k = s_k + n_k$$

where

$$n_k = \frac{1}{\sqrt{P_R}T_C}\int_{(k-1)T_C}^{kT_C} n(t)dt$$

The integral n_k is a Gaussian random variable with zero mean.

Since

$$\mathrm{E}\left[\int_{(k-1)T_C}^{kT_C} n(t_1)dt_1 \int_{(k-1)T_C}^{kT_C} n(t_2)dt_2\right] = \int_{(k-1)T_C}^{kT_C}\int_{(k-1)T_C}^{kT_C} \mathrm{E}\left[n(t_1)n(t_2)\right]dt_1dt_2$$

$$= \int_{(k-1)T_C}^{kT_C}\int_{(k-1)T_C}^{kT_C} \frac{N_0}{2}\delta(t_1 - t_2)\,dt_1dt_2 = \int_{(k-1)T_C}^{kT_C} \frac{N_0}{2}\,dt_2 = \frac{N_0}{2}T_C$$

where E[.] denotes the expectation operator, n_k is also a zero-mean Gaussian random variable with variance:

$$\left(\frac{1}{\sqrt{P_R T_C}}\right)^2 \frac{N_0}{2} T_C = \frac{N_0}{2P_R T_C} = \frac{N_0}{2E_C}$$

where $E_C = P_R T_C$ is the *chip energy*. Because $|s_k|^2 \equiv 1$, it follows that the *chip SNR* is

$$\mathrm{SNR}_{\mathrm{chip}} = \frac{2P_R T_C}{N_0} = \frac{2E_C}{N_0}$$

Because the range-clock fundamental frequency is

$$f_{RC} = \frac{1}{2T_C}$$

the chip SNR can also be written as

$$\mathrm{SNR}_{\mathrm{chip}} = \frac{P_R}{N_0} \cdot \frac{1}{f_{RC}}$$

2.4.3.1.3 Acquisition Probability

The probing sequence C_i will be correctly acquired if and only if its in-phase cyclic shift would win a pairwise contest with each of the L_i-1 out-of-phase cyclic shifts of the probing sequence. The *probability of error* P_{eLi} in *acquiring this probing sequence* is thus very well approximated as:

$$P_{eLi} \approx (L_i\text{-}1)P_{e2}$$

when P_{e2} is small. The right side of this equation is always a strict upper bound on P_{eLi} and is also a good approximation of P_{eLi} since the events that the in-phase cyclic shift wins the individual pairwise contests are substantially independent so that:

$$1 - P_{eLi} = (1 - P_{e2})^{Li\text{-}1} \approx 1 - (L_i\text{-}1)P_{e2}$$

From the above equation it can be seen that the probing sequence C_6 has the greatest probability of acquisition error, but its acquisition time is more than 20% longer than that of the other probing sequences. Assuming that all six probing sequences are correlated in parallel and that the correlation time is the one defined by C_6, it can be concluded that the probabilities of error in acquiring the other five probing sequences will be much smaller. It follows that correlating all six probing sequences in parallel over the required correlation time for probing sequence C_6, makes it possible to neglect the probability of erroneous acquisition of the other five probing sequences and conclude that

$$P_{ACQ} \approx 1 - P_{e23} \approx 0.999$$

which is the target probability of successful acquisition. This results in $P_{e23} \approx 1.1\times10^{-3}$. Since the integraton time for C_6 is also used for the other sequences, P_{eLi} will decrease progressively from C_5 to C_1.

2.4.3.2 Accurate Analysis

A more accurate analysis for the on-board acquisition performances is based on the same approach applied in 2.6.3.2 for the ground station case.

$$P(C_i) = \int_{-\infty}^{\infty}\left[1-\frac{1}{2}erfc(y)\right]^{L_i-1}\cdot\sqrt{\frac{1}{\pi}}\exp\left[-\left(y-\sqrt{\gamma}\right)^2\right]dy$$

where $P(C_i)$ is the probability of correct decision on each code C_i and

$$P_{ACQ}(C)\cong\prod_{i=1}^{6}P(C_i)$$

$$erfc(x)=1-erf(x)$$

$$erf(x)=\frac{2}{\sqrt{\pi}}\int_0^x e^{-t^2}dt$$

However, for the on-board mixed serial/parallel architecture, since each probing sequence C_i is acquired using a serial algorithm, the noise component for the L_i different correlations can be assumed statistically independent[3]. Therefore, in this case

$$\sigma_\eta^2=\frac{N_0}{2}T_{COR}$$

and

$$\gamma=\left(\frac{\rho^*_{i0}-\rho^*_{i1}}{L}\right)^2\frac{E_c}{N_0}\frac{T_{COR}}{T_c}=\left(\frac{\rho^*_{i0}-\rho^*_{i1}}{L}\right)^2\frac{P_R}{N_0}T_{COR}$$

where ρ^*_{ik} are the normalized correlation coefficients defined in 2.6.3.2.

For the on-board receiver, it can be observed that the correlation time for code C_i is $T_{COR,i} = T_{ACQ}/L_i$, since L_i phases are serially processed in the time interval T_{ACQ}. As an example, the correlation time applied for code C_2 is 23/7 of the correlation time of the code C_6 and as a consequence $P(C_2) >> P(C_6)$. So one can conclude that for the on-board acquisition scheme $P_{ACQ} \approx P(C_6)$, and $T_{ACQ} = 23\times T_{COR6}$. The required correlation time T_{COR6} for a probability of

[3] This is the reason why the simplified analysis and the accurate analysis provide similar results for on-board applications when the serial algorithm is applied for each probing sequence C_i.

successful acquisition P_{ACQ} equal to 99.9 % is obtained by inverting the second equation in this subsection but practically the same results are obtained by inverting the first one with i = 6 (the relative error is lower than 0.3% for this P_{ACQ} value).

2.4.3.3 Simplified versus Accurate Analysis

The theoretical acquisition time values specified in the Blue Book have been derived using the expressions and procedure reported in 2.4.3.2.

However, following the simplified approach of 2.4.3.1 and observing that

- the values of table 2-7 are related to $2E_c/N_0$=-33 dB or P_R/N_0=27 dBHz, and
- the acquisition time at 30 dBHz is one half of the acquisition time at 27 dBHz,

one finds 87.8 s for T4B and 5.3 s for T2B. This corresponds to an error of about 2% when compared with the accurate analysis results. It must be underlined that the simplified analysis is correct from a theoretical point of view,[4] but because of some approximations in the calculations there is such small discrepancy in the final result. However, it is very useful since it allows finding a final closed expression for the acquisition time showing the impacts due to the SNR and the code coefficients ξ and ψ.

2.4.4 ON-BOARD H/W IMPLEMENTATIONS AND LIMITATIONS

The theoretical evaluations reported in 2.4.2 and 2.4.3 are based on a set of assumptions reported in 2.4.1, in particular:

- No quantization effects at the matched filter output.
- Code detection implemented using the maximum search algorithm.

In order to limit the DSP complexity the number of bits for signal representation at the matched filter output must be properly limited. The hard quantization (1 bit only) clearly minimizes the gate number but introduces additional losses in the acquisition performances. The 3-bit quantization represents a good compromise in terms of performances versus complexity.

The algorithm based on the maximum search represents the optimum approach (in terms of acquisition performances) for PN signal acquisition. However, this algorithm shows a limitation: also in absence of a useful input signal (i.e., with noise only) it will find a maximum.

It is true that code acquisition is executed after the CTL has declared the lock condition, but a false CTL lock could generate a false PN acquisition. To minimize this false probability one of the following approaches can be applied (for each of the C_i sequences):

[4] This is not true for the station acquisition performances when implementing full parallel receiver.

a) Approach Based on Confirmation of the Acquisition

Different solutions can be proposed, for instance:

– to confirm the PN code acquisition comparing the selected maximum value with a predefined threshold (including S+N normalization using a dedicated ranging AGC);

– to confirm the PN code acquisition checking the difference (in amplitude) between the selected maximum value and the other Li-1 values: acquisition confirmed if the difference is bigger than a predefined threshold;

– entering the tracking mode and continuously checking if the acquired code phase corresponds to the maximum for each C_i codes; PN acquisition could be declared achieved after some confirmations, for instance n success over k trials.

b) Approach Based on Proper Link Procedure

– to apply the ranging modulation on the uplink signal before enabling the on-board ranging channel: in this way the ranging processor never processes the noise alone.

For the first approach the acquisition process is (in practice) terminated when confirmation has been achieved; only at this point the turnaround function can be enabled with the application of the regenerated PN ranging signal at the downlink modulator.

An additional approach could be to replace the maximum search algorithm with the fixed threshold comparison. Of course, to optimize the performances versus different input signal power levels, S+N normalization using a dedicated ranging AGC is required. However, in the usual case where the in-phase cyclic shift is orthogonal (or nearly so as in figure 2-12) to the out-of-phase cyclic shift, the squared length of the line segment CB is twice (or nearly so) the squared length of the line segment CD. This means that one pays approximately 3 dB penalty in the required SNR to achieve a specified performance when one uses the best fixed-threshold decision rule instead of the optimum decision rule (i.e., maximum search). Only for antipodal signals (i.e., the clock component) there is no loss when using the best fixed-threshold decision rule.

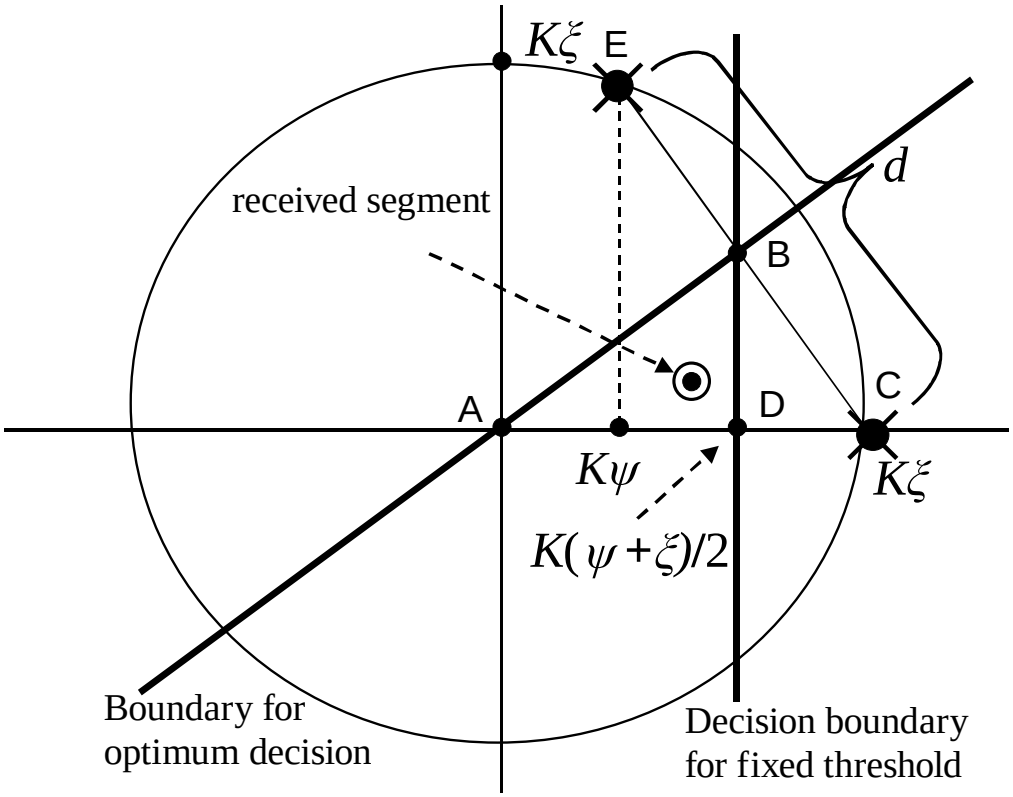

Optimum Decision Boundary = Maximum Search

Figure 2-12: Space Representation for the Probe Sequence C_i and Decision Boundaries

In case of fixed threshold comparison, the threshold shall be defined considering the correct acquisition but also the false acquisition (for out-of phase correlation) probability.

The comparison between the maximum search and the Threshold Comparison acquisition procedures is shown in table 2-8 in terms of a loss in dB for the same acquisition probability (P_{ACQ} =P_{ACQ_equiv}= 99.9%). The loss for the three cases of threshold comparison is defined as the required additional dB with respect to a P_R/N_0 = 27 dBHz in order to have the maximum acquisition time obtained by Threshold Comparison equal to the acquisition time obtained by the maximum search (see reference [13]).

Table 2-8: Maximum Search versus Threshold Comparison Acquisition Procedure

		Maximum Search	Threshold Comparison		
		Ideal Processing No Quantization	Ideal Processing No Quantization	Ideal Processing 3-bit Quantization	Ideal Processing 1-bit Quantization
T2B	Acquisition Time (s)	10.6	21.5	22.9	33.8
	Loss (dB)		3.1	3.4	5.1
T4B	Acquisition Time (s)	175.6	358.2	381.0	562.7
	Loss (dB)		3.1	3.4	5.1

Clearly the impact due to one-bit quantization is around 2 dB when compared to the non-quantized case while three-bit soft quantization reduces this loss down to 0.3 dB only.

2.5 ON-BOARD PN TRACKING JITTER

2.5.1 SQUARE-SQUARE MATCHED CASE

The PN ranging code resembles a square-wave with a few 'errors'. Therefore the CTL can be simply designed by modifying a DTTL according to figure 2-13. The filtered loop error is added to the nominal chip rate and the result is used to control the NCO frequency. The ranging signal clock component is coherently related to the transmitted carrier frequency; therefore it is possible to apply an aided acquisition scheme for proper CTL synchronization. With this approach, the chip rate is obtained by adding the nominal chip rate to the carrier loop error scaled by the ratio of the ranging chip rate by the uplink carrier frequency. This second term offers an estimation of the Doppler on the ranging signal and allows improving the CTL acquisition performance because only the chip phase (not the frequency) must be recovered. The CTL NCO output frequency is used to drive the shift registers which generate the six code components in the Code Generator blocks.

The signal at the CTL input is derived from the carrier quadrature channel and it can be expressed as:

$$r(i) = r(it_s) = A\sum_k a_k \cdot p(it_s - kT - \tau) + N_i$$

where:

t_s is the sampling interval;

A is the amplitude of the chip;

$T = T_c$ is the chip period;

N_i is zero mean white Gaussian noise sample with variance:

$$\sigma_i^2 = \frac{N_0}{2t_s}$$

τ is the random epoch to be estimated;

$p(t_i)$ is the square-wave function having a value of 1 for $0 \le t_i \le T$ and having value 0 elsewhere, i.e.:

$$p(it_s) = \text{rect}\left(\frac{it_s}{T}\right)$$

a_k represents the k_{th} chip polarity.

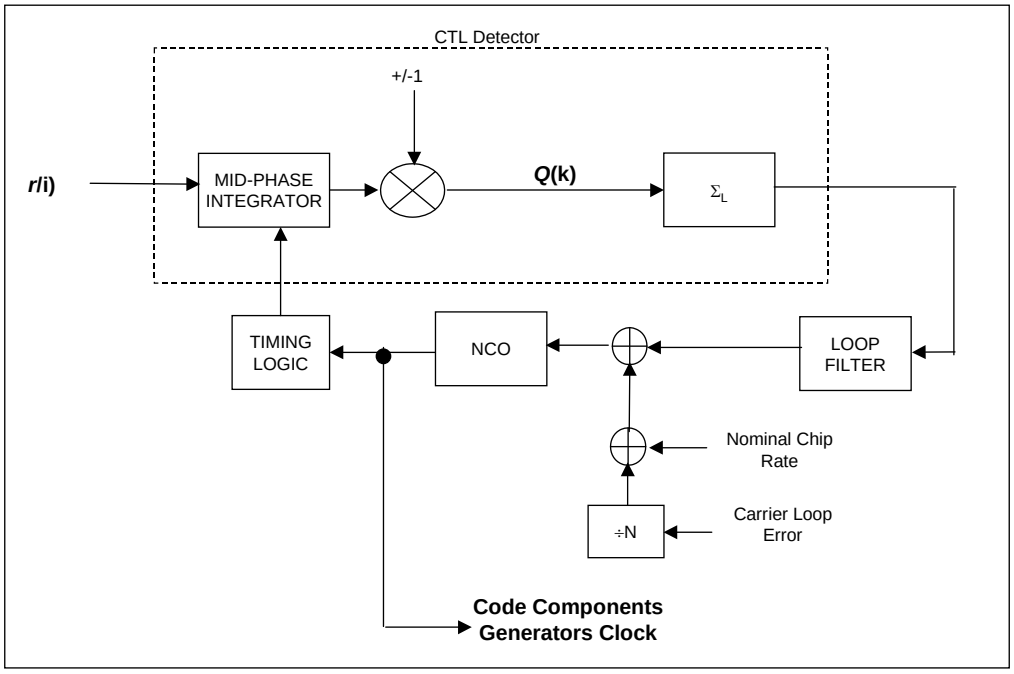

Figure 2-13: CTL Block Diagram

In this way it is possible to consider, at the CTL input, a square-wave shaped signal; the mid-phase integrator (based on a Integrate and Dump approach) represents a solution matched to the signal for the phase error estimation.

It can be assumed that the input symbols have their leading edge at $\ldots kT + \tau, (k+1)T + \tau, \ldots$, and that the loop generates its leading edges at $\ldots kT + \hat{\tau}, (k+1)T + \hat{\tau}, \ldots$so the timing error ε is:

$$\varepsilon = \tau - \hat{\tau}$$

Now the tracking performance of the CTL in terms of timing jitter, namely σ_ε^2., can be determined.

Using linear theory, σ_ε^2 can be derived once the following two quantities are determined:

a) the loop *S*-curve;

b) the two-sided spectral density of the equivalent additive noise.

The *S*-curve is defined as the mean value of the error control signal conditioned on the timing error. Mathematically:

$$S(\varepsilon) = L \cdot E(Q_k | \varepsilon)$$

where $E(\bullet)$ denotes the statistical expectation, $Q_k = Q(k)$ is the quadrature channel output (see figure 2-13) and L represents the accumulation length of the integrate-&-dump following the quadrature branch of the CTL. The mid-phase integrator output is given by (see figure 2-14):

$$Q_k = \sum_{i \in C_k} r(i) = \sum_{i \in C_k} \{A[a_k \cdot p(it_s - kT - \tau)] + N_i\}$$

where:

$$C_k = \left\{ i : \left(k - \frac{1}{2}\right)T + \hat{\tau} \le it_s < \left(k + \frac{1}{2}\right)T + \hat{\tau} \right\}$$

The mid-phase integrator output is multiplied by ±1 in order to provide the right correction to the loop. In a certain way the multiplication by ±1 replaces the transition detector considering that the PN sequence resembles a square-wave. The mean value of the mid-phase integrator output after multiplication by +1/-1 is easily found:

$$E(Q_k) = 2A \cdot \left(\frac{\varepsilon}{t_s}\right)$$

$$S(\varepsilon) = 2AL\left(\frac{\varepsilon}{t_s}\right)$$

The obtained relationship for the *S*-curve is meaningful when the loop is tracking. Besides, because of the nature of the accumulation, ε is always quantized to an integer multiple of the sampling period t_s; however, the presence of noise makes the quantization effect negligible, if the number of samples per chip is high enough. The slope of the *S*-curve at the origin represents the loop detector gain K_ε:

$$K_\varepsilon = \left.\frac{\partial S(\varepsilon)}{\partial \varepsilon}\right|_{\varepsilon=0} = \frac{2AL}{t_s}$$

To evaluate the loop equivalent additive noise, it is assumed the CTL is tracking ($\varepsilon \to 0$). Under this assumption the variance at the phase detector output is:

$$\sigma_N^2 = L \cdot \mathrm{Var}(Q_k) = L\frac{N_0}{2t_s}\left(\frac{T}{t_s}\right) = L \cdot \frac{N_0 T}{2t_s^2}$$

The loop timing jitter σ_ε^2 can be estimated using a linearized model of the CTL. With this approach, the loop error η at the phase detector output can be written as:

$$\eta = K_\varepsilon \cdot \varepsilon + N$$

being N the additive Gaussian noise. The above relationship leads to the equivalent linearized loop reported in figure 2-15.

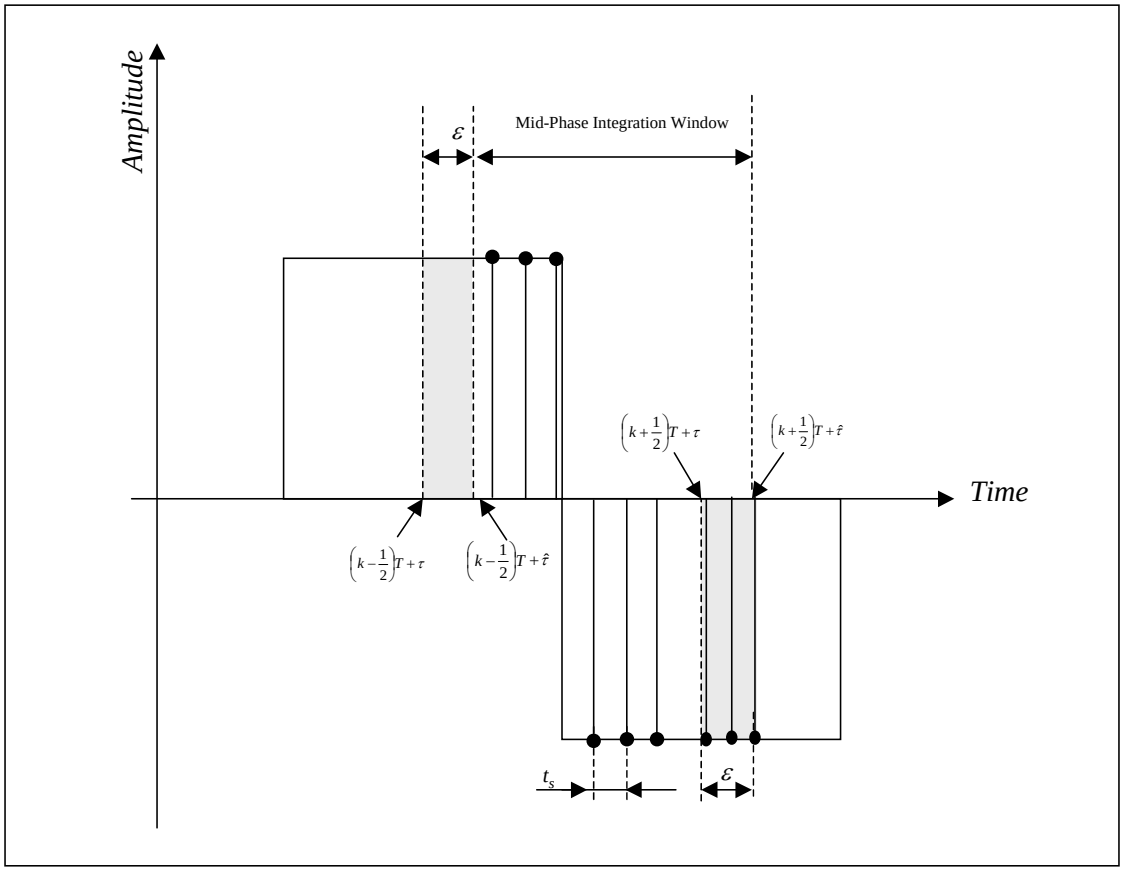

Figure 2-14: Mid-Phase Integration

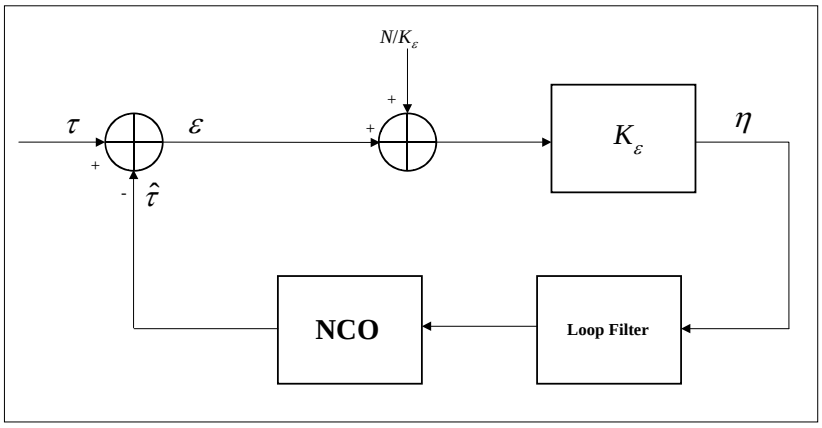

Figure 2-15: Linearized Loop Model (Synchronization Error Expressed As Timing Error)

Using the linearized model:

$$\sigma_{\varepsilon}^{2} = \frac{\left(\frac{S_N}{2}\right) \cdot 2B_L}{K_{\varepsilon}^{2}}$$

where B_L is the one-side loop bandwidth and S_N is the spectral density of the additive noise in the loop, that is:

$$\frac{S_N}{2} = \sigma_N^2 \cdot (L \cdot T) = L^2 \cdot \frac{N_0 T^2}{2t_s^2}$$

and

$$\sigma_{\varepsilon}^{2} = \frac{\left(L^2 \cdot \frac{N_0 T^2}{2t_s^2}\right) \cdot (2B_L)}{\left(\frac{2AL}{t_s}\right)^2}$$

from which:

$$\sigma_{\varepsilon}^{2} = \frac{1}{4} \cdot \frac{B_L \cdot T^2}{(P_R / N_0)}$$

where $\frac{P_R}{N_0} = \frac{1}{T} \cdot \frac{E_c}{N_0}$ is the ranging power-over-noise spectral density ratio, being E_c/N_0 equal to A^2T (i.e., $P_R=A^2$).

In the above calculation it has been assumed all the power of the ranging signal as useful power for the CTL, but in reality, because of the CTL filtering action, only the clock component is used for the tracking of the chip rate. So, replacing the ranging power P_R with the power associated to the clock component P_{RC} and considering that the frequency of the ranging clock component f_{RC} is half of the chip rate value ($F_C = 1/T_c = 2f_{RC}$):

$$\sigma_\varepsilon = \frac{1}{4 f_{RC}} \cdot \sqrt{\frac{B_L N_o}{P_{RC}}} \qquad \text{[s]}$$

Finally, the one-way ranging jitter can be written as:

$$\sigma_{Range\_CTL\_sq\_sq} = \frac{c}{2}\sigma_\varepsilon = \frac{c}{8 f_{RC}} \cdot \sqrt{\frac{B_L}{(P_{RC}/N_0)}} \qquad \text{[m]}$$

being c the speed of the light.

2.5.2 SINE-SQUARE MISMATCHED CASE

It must be underlined that the above analysis is based on a square-wave shaped signal and a matched receiver; in most of the cases the channel (in particular the transmit and the receive analogue front-ends) implements a filtering action removing the higher code (and ranging clock) components. For instance, assuming a chip rate of 3 Mc/s and a receiver with approximately an IF bandwidth of 6 MHz, all the clock spectral components of order higher than 1 are strongly affected by filtering action. As worst case one can consider that, because of this filtering, the ranging sequence appears as sine-wave shaped at the CTL input. In this case, assuming just the fundamental clock component, one has to consider additional power loss and SNR reduction at demodulator input (resulting from the RF front-end). For instance, one has to remember that 81% of the overall power of square-wave signal is related to the fundamental or first component.

However, in the following an ideal sine-wave shaped ranging signal (neglecting the losses due to channel filtering) is considered, and focus is on the CTL performances.

In this case the expression for the S curve above provided (see 2.5.1) is not valid anymore. To evaluate it, as in figure 2-14, two consecutive chips of different polarity sine-waved shaped with amplitude $\sqrt{2}A$ are considered: this corresponds to a sinusoidal signal clock of power A^2. Again a synchronization error is assumed (in the square-shaped Mid-phase integration) equal to ε:

$$\sqrt{2}A \sum_{K}^{(N/2)+K} \cos\left(2\pi \cdot n \frac{t_s}{T}\right) \approx 2\sqrt{2}A \frac{\varepsilon}{t_s}$$

where $\varepsilon = Kt_s$ and $T = Nt_s$. The above approximation is valid in tracking in case of small errors ε. Therefore:

$$E(Q_k) = 2\sqrt{2}A \cdot \left(\frac{\varepsilon}{t_s}\right)$$

$$S(\varepsilon) = 2\sqrt{2}AL\left(\frac{\varepsilon}{t_s}\right)$$

$$K_\varepsilon = \left.\frac{\partial S(\varepsilon)}{\partial \varepsilon}\right|_{\varepsilon=0} = 2\frac{\sqrt{2}AL}{t_s}$$

Considering that for the noise terms the same equations of the square-matched case and applying the same considerations for the ranging clock power and the ranging clock frequency:

$$\sigma_\varepsilon = \frac{1}{\sqrt{2}}\frac{1}{4f_{RC}} \cdot \sqrt{\frac{B_L N_o}{P_{RC}}} \qquad \text{(s)}$$

Finally, the one-way ranging jitter can be written as:

$$\sigma_{Range\_CTL\_\sin\_sq} = \frac{c}{2}\sigma_\varepsilon = \frac{1}{\sqrt{2}}\frac{c}{8f_{RC}} \cdot \sqrt{\frac{B_L}{(P_{RC}/N_0)}} \qquad \text{[m]}$$

2.5.3 COMPARISON OF SINE AND SQUARE SHAPING PERFORMANCE

As described and derived in 2.5.1 the performances of the CTL expressed in terms of time tracking jitter $\left(\sigma_{\varepsilon\_sq\_sq}\right)$ are:

$$\sigma_{\varepsilon\_sq\_sq} = \frac{1}{4f_{RC}} \cdot \sqrt{\frac{B_L N_o}{P_{RC}}} \qquad \text{[s]}$$

where:

- f_{RC} is the frequency of the ranging clock (half of the chip rate value), (Hz);
- P_{RC} is the power of the ranging clock component (square-wave in this case) at CTL input (W);
- N_0 is the one-sided noise power spectral density (W/Hz) at CTL input;
- B_L is the one-sided loop noise bandwidth of the CTL (Hz).

This expression is related to the square-wave signal and matched receiver (square-shaped integrated and dump filtering for the Mid-phase integrator) under the following conditions:

- ideal CTL;

– no impacts due to time quantization (number of samples per chip);

– soft quantization of the chip detection filter (matched filter);

– no interference contribution due to telecommand.

For the one-way ranging rms error:

$$\sigma_{Range\_CTL\_sq\_sq} = \frac{c}{8 f_{RC}} \cdot \sqrt{\frac{B_L}{(P_{RC}/N_0)}} \qquad [\text{m}]$$

where c is the speed of the light (m/s).

In case of sine-wave shaped ranging sequence (see 2.5.2) and assuming the same ideal conditions above mentioned, the CTL performances (still implemented using a square-wave shaped Mid-Phase integrator) become:

$$\sigma_{\varepsilon\_\sin e\_sq} = \frac{1}{\sqrt{2}} \frac{1}{4 f_{RC}} \cdot \sqrt{\frac{B_L N_o}{P_{RC}}} \qquad [\text{s}]$$

$$\sigma_{Range\_CTL\_\sin e\_sq} = \frac{1}{\sqrt{2}} \frac{c}{8 f_{RC}} \cdot \sqrt{\frac{B_L}{(P_{RC}/N_0)}} \qquad [\text{m}]$$

where P_{RC} is the power of the sinusoidal clock component at CTL input.

Therefore the following relation exists:

$$\sigma_{\varepsilon\_\sin e\_sq} = \frac{\sigma_{\varepsilon\_sq\_sq}}{\sqrt{2}}$$

The sine-square expression are applicable in case of sine-wave shaped signal in transmission, but can be applied also (as limit condition) for the situation when the square-wave shaped transmitted signal is strongly filtered in the receiver side before the CTL. In the latter case, the expression takes into account only the performances of the CTL and neglects any contribution (in terms of degradation) due to the channel filtering. Indeed in the above expressions P_{RC}/N_0 represents the power of the ranging clock (assumed sinusoidal as limit case) over noise spectral density at the CTL input.

As derived in 2.7.2.3, the one-way ranging rms error for the case of sinewave shaping with matched receiver is:

$$\sigma_{Range\_CTL\_\sin e\_sne} = \frac{1}{4\pi} \frac{c}{f_{RC}} \cdot \sqrt{\frac{B_L}{(P_{RC}/N_0)}} \qquad [\text{m}]$$

In the same conditions indicated in the Blue Book, the following is obtained:

- B_L=1 Hz;
- chip rate F_c = 2.068 Mchip/s (f_{RC}= F_c/2);
- P_R/N_0 =30 dBHz:

  a) T4B: $P_{RC}/N_0 = P_R/N_0 - 20LOG_{10}(\xi_1) \approx 29.45$ dBHz;

  b) T2B: $P_{RC}/N_0 = P_R/N_0 - 20LOG_{10}(\xi_1) \approx 25.95$ dBHz.

And finally:

Table 2-9: Station Ranging Jitter Performances

Sequence	$\sigma_{Range\_CTL\_sine\_sine}$	$\sigma_{Range\_CTL\_sine\_sq}$	$\sigma_{Range\_CTL\_sq\_sq}$
T4B	0.78 m	0.87 m	1.22 m
T2B	1.17 m	1.29 m	1.82 m

As above underlined, the expressions for the on-board tracking jitter are relevant to a theoretical CTL behavior; for this reason the Blue Book specifies in addition a value of 2 dB for the implementation losses. These losses take into account the contributions due to signal quantization and non-perfect carrier tracking and signal demodulation.

Concerning the signal quantization effects: the signal amplitude quantization (in terms of number of bit), the time sampling (i.e., finite number of samples per chip) and the chip asymmetry.

The effects due to amplitude quantization and the chip asymmetry can be considered in general negligible. Different is the situation for the time sampling. Taking into account that the sampling frequency is equal to F_S, this contribution ($\sigma_{\varepsilon Q}$) can be estimated as:

$$\sigma_{\varepsilon Q} = \frac{1}{\sqrt{12}} \frac{1}{F_S} \quad \text{(s)}$$

For instance, at F_S = 20 MHz there is an rms error of 14 ns (2.1 m one-way), bigger than the theoretical values related to the thermal noise at P_R/N_0=30 dBHz and for B_L=1 Hz.
Concerning the time sampling contribution:

- it is constant and independent from the signal to noise ratio'
- at low loop SNR, it is masked by the jitter due to the thermal noise;
- as the thermal jitter, it can be reduced with average processing at ground station.

Finally the Blue Book (reference [1]) specifies as reference point for the on-board ranging jitter the theoretical performances for a CTL loop bandwidth B_L of 1Hz. In case of wider on-board loop bandwidth[5] implementation, the theoretical jitter values can be recalculated using the following expression:

$$\sigma_{B_L} = \sigma_{1Hz}\sqrt{B_L}$$

The implementation loss smaller than 2 dB shall be referred to these new theoretical jitter values.

2.6 STATION ACQUISITION

2.6.1 INTRODUCTION

The theoretical on-board acquisition time and the analysis reported in this subsection are based on an ideal linear channel and a station processing implementing:

a) full parallel approach based on 76 parallel correlators;

b) maximum search algorithm;

NOTE – It is shown (see on-board analysis in 2.4.4) that the maximum search corresponds to the optimum receiver solution.

c) perfect carrier demodulation (the carrier tracking loop jitter degradation is not considered);

d) perfect chip tracking (the CTL jitter degradation is not considered);

e) no impacts due to amplitude quantization of the signal at the output of the chip detection filter (matched filter);

f) no impacts due to time quantization (number of samples per chip).

In addition the degradation due to downlink telemetry interference (although negligible) is not considered in this analysis, it is reported in 2.8.

2.6.2 STATION DSP ARCHITECTURE FOR PN RANGING PROCESSING

The Station PN ranging operations are accomplished in two stages: first the received ranging clock component is acquired and once this has taken place, the ranging code position is searched, acquired, and tracked.[6]

[5] The specification for the on-board CTL loop bandwidth is mission dependent.
[6] For the end-to-end delay measurement with the comparison between the transmitted (uplink) and received (downlink) code epoch.

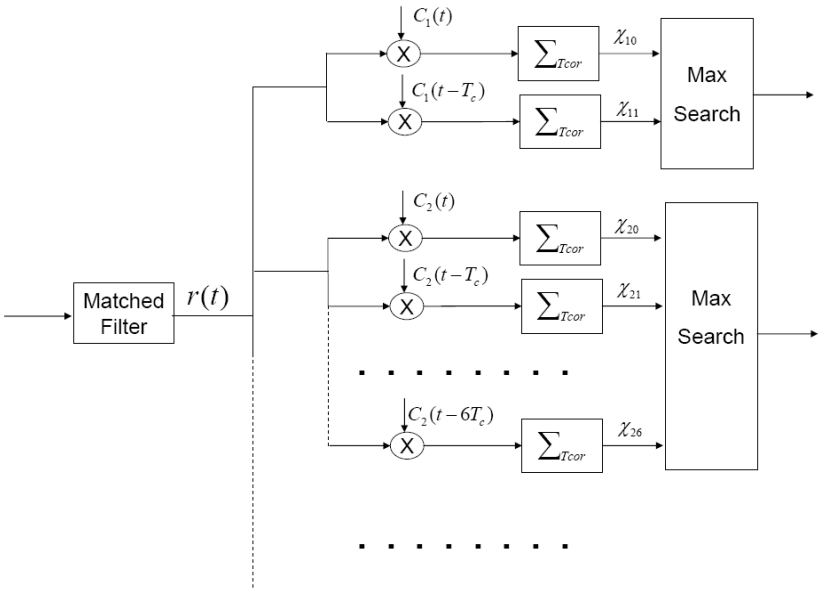

Figure 2-16: Station Architecture for PN Ranging Acquisition Processing (Fully Parallel Approach)

The code phase acquisition process can be carried out by using a bank of correlators to perform in parallel all the correlations against each possible cyclic shift of each probing sequence (see figure 2-16). The total number of correlations required is thus $\sum_i L_i = 77$.

In practice this means a total of 76 correlators since the cyclic shift of the range clock is simply the negative of itself and only one correlator is needed to confirm the correct C1 phase as recovered by the CTL. Once code phase acquisition is completed, it is possible to evaluate the round-trip delay from the estimated probing sequence phases using the Chinese remainder theorem (reference [7]).

In this full parallel case, the ranging sequence acquisition time $T_{ACQ\_G/S}$ at the *G*/*S* (= ground station) simply equals the longest time (among the different probing sequences) to perform the correlation with the desired error probability.

2.6.3 PERFORMANCE EVALUATION

2.6.3.1 Simplified Analysis

Making reference to the full parallel approach described in 2.6.2 and applying the results of the simplified analysis for the evaluation of the on-board acquisition performances of 2.4.3.1, the following can be written (see references [2] and [5]):

$$T_{ACQ\_G/S} = MAX_i \left\{ \frac{\left[Q^{-1}(P_{e2})\right]^2}{2 \cdot \frac{P_r}{N_0}} \times \frac{1}{\xi_i \cdot \left(\frac{\xi_i - \psi_i}{2} \right)} \right\}$$

This closed form expression represents only an approximation for the station acqusition time[7]. In particular, for the derivation of this expression, the noise terms at the correlator output are assumed statistically independent (among the different correlators of the full parallel scheme). This is not true.

The above equation indicates that $T_{ACQ\_G/S}$ is shorter than $T_{ACQ\_S/C}$ by a factor L_6 for the same $P_{R/}N_0$.

Assuming the correlator outputs as statistically independent for this parallel acquisition strategy, the probability of successful acquisition can be approximated by $P_{ACQ} \approx 1\text{-}22 \cdot P_{e2}$.

2.6.3.2 Accurate Analysis

As indicated in 2.6.2, the acquisition process consists in finding the correct phase of the probing sequences C_i by correlating the received signal $r(t)$ (combination of PN ranging signal $S(t)$ plus noise $n(t)$) against a local model of each probing sequence C_i and all of its cyclic shifts. The correlation χ_{ik} for time T_{COR} against the *k-th* shift of code C_i can be described as:

$$\chi_{ik} = \int_0^{T_{COR}} r(t) \cdot C_i(t - kT_c)dt = \int_0^{T_{COR}} S(t) \cdot C_i(t - kT_c)dt + \int_0^{T_{COR}} n(t) \cdot C_i(t - kT_c)dt = \rho_{ik} + \eta_{ik}$$

The shift by k chips (k = 0, 1, 2,…, L_i-1) that gives the greatest correlation value χ_{ik} is selected as the one which is in-phase with the received sequence. While η_{ik} is merely the noise contribution at the correlator output, the component ρ_{ik} represent the correlation value of the received *PN* sequence $S(t)$ with a unit amplitude and shifted version of C_i after the correlation time T_{COR}. Assuming a ranging signal power $P_R = E_c/T_c$, the coefficients ρ_{ik} can be calculated as

[7] The analysis behind this expression provides good performances estimation for the on-board mixed parallel/serial approach.

$$\rho_{ik} = \sqrt{\frac{E_c}{T_c}} \cdot \int_0^{T_{COR}} s(t) \cdot C_i(t - kT_c)dt = \sqrt{E_c T_c} \cdot \rho^*_{ik} \cdot \frac{T_{COR}}{T_r}$$

where:

– $S(t) = \sqrt{\frac{E_c}{T_c}} \cdot s(t)$ and $s(t) = s_k$ for $(k-1)T_C < t \le kT_C$ are the binary (±1) ranging-sequence waveform with chip values $s_k \in \{+1, -1\}$;

– T_C is the chip duration;

– $T_r = LT_c$ is one sequence length;

– ρ^*_{ik} are the normalized correlation coefficients (i.e., unit amplitude and correlation time equal to one sequence length $T_r = LT_c$).

As indicated in table 2-10, the normalized correlation coefficients are related to the in-phase (ξ) and out-of-phase (ψ) fractional correlation coefficient as defined in 2.4.3

Table 2-10: Normalized Correlation Coefficients (Unit amplitude and Correlation Time Equal to One Sequence Length T_r)

	$\rho^*_{10}=L\xi_1$	$\rho^*_{11}=L\psi_1$	$\rho^*_{20}=L\xi_2$	$\rho^*_{2k}=L\psi_2$ (k =1..6)	$\rho^*_{30}=L\xi_3$	$\rho^*_{3k}=L\psi_3$ (k=1..10)
T2B	633306	- 633306	247020	- 41404	250404	- 24900
T4B	947566	- 947566	61904	- 10368	61904	- 6160

	$\rho^*_{40}=L\xi_4$	$\rho^*_{4k}=L\psi_4$ k = 1..14	$\rho^*_{50}=L\xi_5$	$\rho^*_{5k}L\psi_5$ (k =1..18)	$\rho^*_{6}=L\xi_6$	$\rho^*_{6k}=L\psi_6$ (k = 1..22)
T2B	251332	- 17852	251604	- 14056	251940	- 11388
T4B	61904	- 4400	61904	- 3456	61904	- 2800

For code C_1, assuming that $k = 0$ is the true phase, the probability of correct decision is simply[8]:

$$P(C_1) = P(\chi_{10} > 0) = P(\rho_{10} + \eta_{10} > 0) = 1 - \frac{1}{2} erfc\left(\rho^*_{10} \cdot \frac{T_{COR}}{T_r} \cdot \sqrt{\frac{E_c T_c}{N_0 T_{COR}}} \right)$$

being η_{10} Gaussian with zero mean and variance $\frac{N_0 T_{COR}}{2}$ [9].

[8] Noting that C_1 is antipodal and that both $k = 0$ and $k = 1$ are equally probable.
[9] The erfc(x) function is defined in section 2.4.3.2.

For i >2 (i.e., for C_2, ... C_6), the random variables η_{ik} are still Gaussian with zero mean and variance $\frac{N_0 T_{COR}}{2}$, but they are no longer independent since $C_{ik}(t) = C_i(t\text{-}kT_c)$ is not orthogonal to $C_{ih}(t)$ for $k \neq h$[10]. However, it is possible to write $C_{ik}(t) = C'_{ik}(t) + b(t)$, with

$$b(t) = \frac{1 \pm \sqrt{L_i + 1}}{L_i} \cdot \sum_{j=0}^{L_i - 1} C_{ij}(t)$$

so that $C'_{ik}(t)$ are now orthogonal. Therefore it is possible to write

$$\chi_{ik} = \int_0^{T_{COR}} r(t) \cdot C_{ik}(t) dt = \rho_{ik} + \eta_{ik}$$

$$\eta_{ik} = \int_0^{T_{COR}} n(t) \cdot \left[C'_{ik} + b(t) \right] dt = \int_0^{T_{COR}} n(t) \cdot C'_{ik} dt + \int_0^{T_{COR}} n(t) \cdot b(t) dt = \eta'_{ik} + \eta$$

being η'_{ik} independent Gaussian random variables with variance:

$$\sigma^2_{\eta'} = \frac{N_0}{2} \left[1 + \frac{1}{L_i} \right] \cdot T_{COR}$$

The probability of correct decision (for the probe sequence C_i) is then given by:[11]

$$\begin{aligned} P(C_i) &= P(\chi_{i0} > \max\{\chi_{i1}, \ldots, \chi_{iL_i - 1}\} / C_{i0}) = P(\rho_{i0} + \eta'_0 > \max\{\rho_{i1} + \eta'_1, \ldots, \rho_{iL_i - 1} + \eta'_{L_i - 1}\}) \\ &= P(\rho_{i0} - \rho_{i1} + \eta'_0 > \max\{\eta'_1, \ldots, \eta'_{L_i - 1}\} \end{aligned}$$

where $\rho_{i2} = \rho_{i3} = \ldots = \rho_{iLi\text{-}1}$ are used.

Noting that the cumulative probability distribution is[12]

$$P\left(\max\{\eta'_1, \ldots, \eta'_{L_i - 1}\} \leq x\right) = P\left(\eta'_1 \leq x\right) P\left(\eta'_2 \leq x\right) \ldots P\left(\eta'_{L_i - 1} \leq x\right) = \left[1 - \frac{1}{2} erfc \frac{x}{\sqrt{2}\sigma_{\eta'}} \right]^{L_i - 1}$$

and that the probability density function of $x = \rho_{i0} - \rho_{i1} + \eta'_0$ is

[10] In addition for the parallel processor of figure 2-16 the same (correlated) input noise sample are processed by the different L_i correlators for the maximum search.

[11] Assuming that $k = 0$, $k = 1 \ldots k = L_i\text{-}1$ are equally probable. In the following to simplify the expressions the double index (i, k) is removed so that $\eta_k = \eta_{ik}$.

[12] The statistical independence of the η'_k noise components is exploited.

$$P(x) = \sqrt{\frac{1}{2\pi\sigma_{\eta'}^2}} \exp\left[-\frac{[x - (\rho_{i0} - \rho_{i1})]^2}{2\sigma_{\eta'}^2} \right]$$

it is possible to write the probability of correct decision on the code phase of sequence C_i as the integral over all possible values of x; i.e.:

$$P(C_i) = \int_{-\infty}^{\infty} \left[1 - \frac{1}{2} erfc \frac{x}{\sqrt{2}\sigma_{\eta'}} \right]^{L_i - 1} \cdot \sqrt{\frac{1}{2\pi\sigma_{\eta'}^2}} \exp\left[-\frac{[x - (\rho_{i0} - \rho_{i1})]^2}{2\sigma_{\eta'}^2} \right] dx$$

with $\rho_{i0,}$ ρ_{i1} and σ'_{η} functions of T_{COR} as given above.

Defining $y = x/\left(\sqrt{2}\sigma_{\eta'}\right)$, $\gamma = (\rho_{i0} - \rho_{i1})^2 \big/ 2\sigma_{\eta'}^2$ one finds:

$$P(C_i) = \int_{-\infty}^{\infty} \left[1 - \frac{1}{2} erfc(y) \right]^{L_i - 1} \cdot \sqrt{\frac{1}{\pi}} \exp\left[-\left(y - \sqrt{\gamma} \right)^2 \right] dy$$

where

$$\gamma = \left(\frac{\rho^*_{i0} - \rho^*_{i1}}{L} \right)^2 \frac{L_i}{L_i + 1} \frac{E_c}{N_0} \frac{T_{COR}}{T_c} = \left(\frac{\rho^*_{i0} - \rho^*_{i1}}{L} \right)^2 \frac{L_i}{L_i + 1} \frac{P_{RNG}}{N_0} T_{COR}$$

Finally the acquisition process of the full PN ranging sequence is completed successfully when all of the local generated probing sequences C_i are in-phase with the received ranging sequence or[13]

$$P_{ACQ}(C) \cong \prod_{i=1}^{6} P(C_i) .$$

For the ground station parallel receiver all the correlations are evaluated for the same amount of time and the acquisition time T_{ACQ} is equal to T_{COR} in the above equations. The required correlation time T_{COR} for a probability of successful acquisition P_{ACQ} equal to 99.9 % is obtained by inverting the equation above.

2.6.3.3 Comparison of Approximate and Accurate Analysis

The theoretical acquisition time values specified in the Blue Book (reference [1]) have been derived using the accurate expressions and procedure reported in 2.6.3.2.

However, following the simplified approach and observing that:

[13] The decisions on the phases of the probing sequences are correlated, but this correlation can be practically neglected.

- the values are related to $2E_c/N_0$= -33 dB or P_R/N_0= 27 dBHz;
- the acquisition time at 30 dBHz is one half of the acquisition time at 27 dBHz;
- the normalized correlation time is longer (maximum) for the C_6 probe sequence, so it defines the overall acquisition time;
- for the fully parallel approach the acquisition time is 1/23 the acquisition time for the on-board case;

one finds 3.87 s for T4B and 0.23 s for T2B at P_R/N_0 of 30 dBHz. This corresponds to an error of about 10% when compared with the accurate analysis results. As above underlined, the simplified analysis is not correct from a theoretical point of view, since it considers that the noise terms at the correlator output are statistically independent (among the different correlators of the full parallel scheme). However, it is very useful since it allows finding a final closed expression for the acquisition time showing the impacts due to the SNR and the code coefficients ξ and ψ.

In practice, the acquisition performance at the station is affected by the on-board non-linearity (reference [8]) which causes a degradation in the correlation coefficients (ξ_i, ψ_i) of the sequence resulting in an increase in the acquisition time. This effect can be equivalently attributed to a decrease of P_R/N_0: simulations show that non-linear system yields an additional loss of about 0.7 dB with very small differences among the various codes. In principle the same applies for the uplink, but as the transmit channel at the station is much more linear, the increase in acquisition time is negligible in this case.

Table 2-11 below shows the comparison between the values computed using the exact formula and the approximation at the reference point of 30 dBHz for the case of 76 correlators.

Table 2-11: Comparison of Results for Station Parallel Receiver

Sequence	**Maximum Tacq at P_R/N_0=30 dBHz (exact formula)**	**Maximum Tacq at P_R/N_0=30 dBHz (approximation)**
Balanced Weighted-voting Tausworthe, ν=4	ideal: 4.31 s	ideal: 3.87 s with 10% increase: 4.26 s
Balanced Weighted-voting Tausworthe, ν=2	ideal: 0.26 s	ideal: 0.23 s with 10% increase: 0.25 s

Additionally, forming the ratio between the on-board and the station acquisition time (exact values) one can see that the gain of the all-parallel receiver is of the order of 20 instead of the factor 23 (equal to the C6 sequence length) used in first approximation.

2.7 STATION AND END-TO-END JITTER

2.7.1 INTRODUCTION

Two different solutions can be implemented for the Station Ranging measurement:

a) the **closed loop approach** based on the CTL as analyzed for the on-board applications in 2.5; the same equations are applicable for station performance evaluation;

b) the **open loop architecture** analyzed in the following 2.7.2.

The theoretical Station Ranging Jitter Performances and the analysis reported in this subsection are based on a processing implementing:

a) soft quantization of the chip detection filter (matched filter);

b) no impacts due to time quantization (number of samples per chip);

c) no interference contribution due to downlink telemetry;

d) no contribution due to on-board (uplink) tracking jitter.

For the end-to-end jitter, the uplink contribution (due to the on-board CTL jitter) must be considered as detailed in 2.7.3.

2.7.2 OPEN LOOP ARCHITECTURE PERFORMANCES

2.7.2.1 General

In the following the Open Loop architecture (suitable for Ground Station applications) is analyzed for the estimation of the ranging delay. It must be underlined that the accurate PN ranging measurement is performed on the ranging clock component comparing (with an I/Q correlator) the phase of the received clock signal with the phase of the local clock replica. So in the following analysis the ranging signal is represented only with its clock component neglecting the other PN terms (used for ambiguity resolution). Three examples will be considered in the following:

a) Sine-Square (Mismatched Case). Ranging clock component sinusoidal (sine-wave shaped signal) and square-wave reference signal at the I/Q demodulator:

$$\sigma_{Range\_OL\_sine\_sq} = \frac{c}{16 f_{RC}} \cdot \sqrt{\frac{N_0}{P_{RC} T}} \qquad [m]$$

b) Sine-Sine (Matched Case). Ranging clock component sinusoidal (sine-wave shaped signal) and sine-wave reference signal at the I/Q demodulator):

$$\sigma_{Range\_OL\_sine\_sine} = \frac{c}{\sqrt{32\pi^2}\, f_{RC}} \cdot \sqrt{\frac{N_0}{P_{RC} T}} \qquad [m]$$

c) Square-Square (Matched Case). Square-wave ranging clock component and square-wave reference signal at the I/Q demodulator:

$$\sigma_{Range\_OL\_sq\_sq} = \frac{c}{16\, f_{RC}} \sqrt{\frac{N_0}{P_{RC} T}} \qquad [m]$$

In the above expressions the same symbolism applied for the on-board CTL is used, but in this case, instead of the loop bandwidth $B_{L,\,is}$ the integration time T on the I/Q branches of the phase correlator. As for the on-board CTL expressions, also in these cases P_{RC}/N_0 represents the ranging clock power over noise spectral density at the I/Q correlator input.

From the above expressions it is observed that:

$$\sigma_{Range\_OL\_sine\_sq} = \sigma_{Range\_OL\_sq\_sq} = \frac{\sqrt{32\pi^2}}{16} \sigma_{Range\_OL\_sine\_sine}$$

with $\dfrac{\sqrt{32\pi^2}}{16} = \dfrac{\pi}{\sqrt{8}} \approx 1.11$.

2.7.2.2 Sine-Square Mismatched Case

The block diagram sketched in figure 2-17 represents the block diagram for the Ranging Demodulation Processing (RDP).

The signal at the RDP input is given by:

$$x(t) = s(t) + n(t) = \underbrace{\sqrt{2C} sin\left[\omega_0 t + m sin\left(\omega_t t + \theta\right)\right]}_{s(t)} + \underbrace{\sqrt{2} n_c(t) \cos\left[\left(\omega_0 + \omega_t\right)t\right] + \sqrt{2} n_s(t) sin\left[\left(\omega_0 + \omega_t\right)t\right]}_{n(t)}$$

where:

– C = carrier power [W];

– ω_0 = carrier frequency [rad/s];

– $\omega_t = 2\pi f_t$ ranging tone frequency [rad/s];

– f_t = ranging tone frequency [Hz];

– m = ranging tone modulation index [rad-pk];

– = ranging tone phase to be estimated [rad].

and $n_c(t)$, $n_s(t)$ are the AWGN quadrature components having noise spectral density equal to $N_0/2$ (i.e., the signal power-over-noise spectral density ratio is equal to C/N_0).

The signal $y(t)$ at the carrier demodulator output is given by:

$$y(t) = 2\sqrt{C}J_1(m)\sin(\omega_t t + \theta) + n_c(t)\cos(\omega_t t) + n_s(t)\sin(\omega_t t)$$

having assumed that the low-pass filter suppresses the higher-order harmonics of the ranging signals.

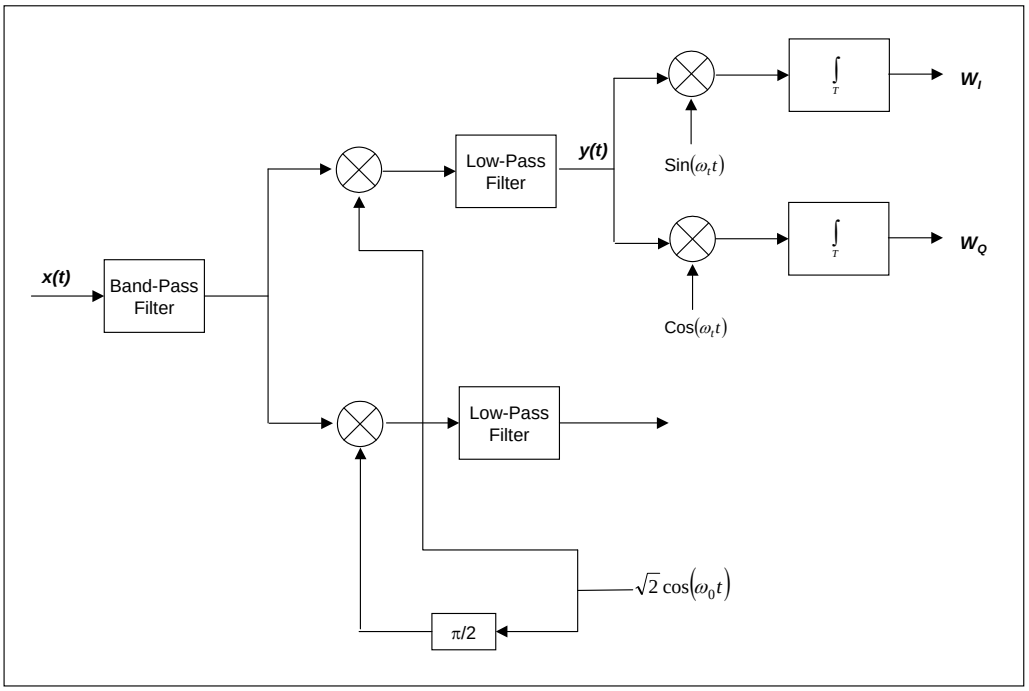

Figure 2-17: Ranging Demodulation Processing: Top-Level Block Diagram

The unknown phase delay θ (see figure 2-17) is estimated evaluating the in-phase W_I and quadrature W_Q components of the $y(t)$ signals as follows:

$$W_I = \int_T y(t) \cdot \mathrm{Sin}(\omega_t t) dt$$

$$W_Q = \int_T y(t) \cdot \mathrm{Cos}(\omega_t t) dt$$

where T is the measurement integration time (in seconds) and:

$$\mathrm{Sin}(x) = \mathrm{sgn}(\sin(x))$$
$$\mathrm{Cos}(x) = \mathrm{sgn}(\cos(x))$$

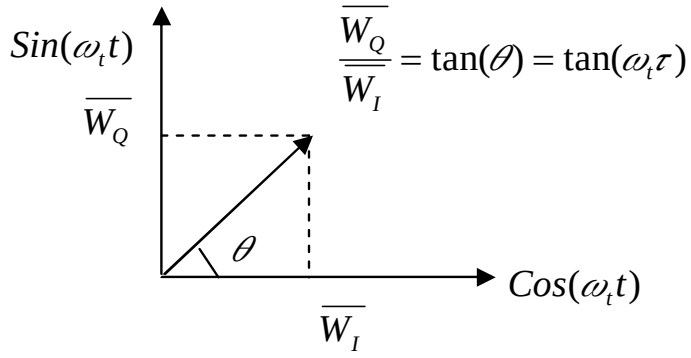

Figure 2-18: Phase Delay Estimation

From the above relationships it is possible to find the average $\overline{W_I}, \overline{W_Q}$ and the standard deviation σ_I, σ_Q of the ranging correlators output, i.e.:

$$\overline{W_I} = \int_T 2\sqrt{C} J_1(m) \sin(\omega_t t + \theta) \cdot \mathrm{Sin}(\omega_t t) dt \approx \int_T 2\sqrt{C} J_1(m) \sin(\omega_t t + \theta) \cdot \frac{4}{\pi} \sin(\omega_t t) dt =$$

$$= \frac{4\sqrt{C}}{\pi} J_1(m) \cos(\theta) T$$

$$\overline{W_Q} = \frac{4\sqrt{C}}{\pi} J_1(m) \sin(\theta) T$$

$$\sigma_I = \sqrt{\frac{N_0}{2} T}$$

$$\sigma_Q = \sqrt{\frac{N_0}{2} T}$$

The two-way ranging delay τ is related to the phase θ by means the following relationship:

$$\tau = \frac{1}{\omega_t} arc \tan\left(\frac{W_Q}{W_I}\right)$$

The standard deviation σ_τ of the two-way ranging delay estimation is given by:

$$\sigma_\tau \approx \left[\left(\frac{\partial \tau}{\partial W_I} \right)^2 \cdot \sigma_I^2 + \left(\frac{\partial \tau}{\partial W_Q} \right)^2 \cdot \sigma_Q^2 \right]^{1/2}$$

being:

$$\frac{\partial \tau}{\partial W_I} = -\frac{1}{\omega_t} \cdot \frac{W_Q}{W_I^2 + W_Q^2}$$

$$\frac{\partial \tau}{\partial W_Q} = \frac{1}{\omega_t} \cdot \frac{W_I}{W_I^2 + W_Q^2}$$

From the above expressions:

$$\sigma_\tau \approx \left[\left(-\frac{1}{\omega_t} \cdot \frac{W_Q}{W_I^2 + W_Q^2} \right)^2 \cdot \frac{N_0}{2} T + \left(\frac{1}{\omega_t} \cdot \frac{W_I}{W_I^2 + W_Q^2} \right)^2 \cdot \frac{N_0}{2} T \right]^{1/2} =$$

$$= \frac{1}{\omega_t} \cdot \sqrt{\frac{N_0 T}{2}} \cdot \frac{1}{\left(W_I^2 + W_Q^2 \right)^{1/2}}$$

Replacing W_I and W_Q with $\overline{W_I}$ and $\overline{W_Q}$ respectively leads to:

$$\sigma_\tau \approx \frac{1}{8 f_t} \cdot \frac{1}{\sqrt{2\left(\frac{C}{N_0} \right) J_1^2(m) \cdot T}}$$

or:

$$\sigma_\tau \approx \frac{1}{8 f_t} \cdot \frac{1}{\sqrt{\left(\frac{P_{RC}}{N_0} \right) \cdot T}} \qquad [\text{s}]$$

where $f_t = \omega_t / 2\pi$ is the ranging tone frequency (also indicated as frequency of the ranging clock f_{RC} for the PN Ranging) and P_{RC}/N_0 is the ranging tone power-over-noise spectral density ratio. Finally, the one-way ranging accuracy can be determined as:

$$\sigma_{Range\_OL\_sine\_sq} = c \cdot \frac{\sigma_\tau}{2} = \frac{c}{16 f_t \cdot \sqrt{\left(\frac{P_{RC}}{N_0} \right) \cdot T}} \qquad [\text{m}]$$

where c is the speed of the light [m/s].

2.7.2.3 Sine-Sine Matched Case

In this case the normalized (unit power) signal references (at the correlator) are

$$\sqrt{2}\cos(\omega_t t)$$

$$\sqrt{2}\sin(\omega_t t)$$

The average value on I and Q branch (at the correlator output) becomes:

$$\overline{W_I} = \overline{\int_T y(t)\cdot\sqrt{2}\sin(\omega_t t)dt} = \sqrt{2C}J_1\cos(\theta)T$$

$$\overline{W_Q} = \overline{\int_T y(t)\cdot\sqrt{2}\cos(\omega_t t)dt} = \sqrt{2C}J_1\sin(\theta)T$$

while it can be shown that, for the standard deviation σ_I and σ_Q, the equations in 2.7.2.2 are still valid. Substituting the above equations in the expression for the rms value:

$$\sigma_\tau \approx \frac{1}{\omega_t}\cdot\sqrt{\frac{N_0T}{2}}\cdot\frac{1}{\left(\overline{W_I}^2+\overline{W_Q}^2\right)^{1/2}} = \frac{1}{2\pi f_t}\sqrt{\frac{N_0T}{2}}\frac{1}{\sqrt{2CJ_1^2T^2}} =$$

$$= \frac{1}{\sqrt{8\pi^2}\,f_t}\sqrt{\frac{N_0}{P_{RC}T}} \qquad [s]$$

The standard deviation of one-way range measurement can be written as:

$$\sigma_{Range\_OL\_sine\_sine} = c\cdot\frac{\sigma_\tau}{2} = \frac{c}{\sqrt{32\pi^2}\,f_t\cdot\sqrt{\left(\frac{P_{RC}}{N_0}\right)\cdot T}} \qquad [m]$$

where c is the speed of the light and f_t is also indicated as f_{RC} (frequency of the ranging clock for the PN Ranging) and P_{RC}/N_0 is the ranging tone power-over-noise spectral density ratio.

$$\sigma_{Range\_OL\_sine\_sine} = \frac{c}{\sqrt{32\pi^2}\,f_t\cdot\sqrt{\left(\frac{P_{RC}}{N_0}\right)\cdot T}} \qquad [m]$$

2.7.2.4 Square-Square Matched Case

In this case the clock is a square wave signal, so the expression of 2.7.2.2 becomes:

$$x(t) = s(t) + n(t) = \underbrace{\sqrt{2C}\,\sin\left[\omega_0 t + m \cdot \mathrm{Sin}(\omega_t t + \theta)\right]}_{s(t)} +$$

$$+ \underbrace{\sqrt{2}n_c(t)\cos\left[(\omega_0 + \omega_t)t\right] + \sqrt{2}n_s(t)\sin\left[(\omega_0 + \omega_t)t\right]}_{n(t)}$$

The signal $y(t)$ at the carrier demodulator output is given by:

$$y(t) = \sqrt{C}\sin(m)\cdot\mathrm{Sin}(\omega_t t + \theta) + n_c(t)\cos(\omega_t t) + n_s(t)\sin(\omega_t t)$$

Developing the above expressions one can find the in-phase and quadrature signal components at the integrator output (see figure 2-18):

$$\overline{W_I} = \int_T \sqrt{2C}\sin(m)\cdot\mathrm{Sin}(\omega_t t + \theta)\cdot\mathrm{Sin}(\omega_t t)dt = \sqrt{C}\sin(m)\cdot T\left[1 - \frac{2\theta}{\pi}\right]$$

$$\overline{W_Q} = \int_T \sqrt{2C}\sin(m)\cdot\mathrm{Sin}(\omega_t t + \theta)\cdot\mathrm{Cos}(\omega_t t)dt = \sqrt{C}\sin(m)\cdot T\left[-\frac{2\theta}{\pi}\right]$$

For the noise, the expressions for the rms value at the integrator output are still valid yielding for the ranging delay $\tau\,(\theta = \omega_t\tau)$:

$$\tau = \frac{\pi}{2\cdot\omega_t}\frac{-\overline{W_Q}}{\overline{W_I} - \overline{W_Q}}$$

and

$$\sigma_\tau \approx \frac{\pi}{2\omega_t}\left[\left(\frac{W_Q}{(W_I - W_Q)^2}\right)^2 \cdot \frac{N_0}{2}T + \left(\cdot\frac{-W_I}{(W_I - W_Q)^2}\right)^2 \cdot \frac{N_0}{2}T\right]^{1/2} =$$

$$= \frac{\pi}{2\omega_t}\sqrt{\frac{N_0}{2}T}\left[\left(\frac{W_Q}{(W_I - W_Q)^2}\right)^2 + \left(\cdot\frac{-W_I}{(W_I - W_Q)^2}\right)^2\right]^{1/2} =$$

$$= \frac{\pi}{2\omega_t}\sqrt{\frac{N_0}{2}T}\,\frac{\sqrt{W_I^2 + W_Q^2}}{(W_I - W_Q)^2}$$

where:

$$\left(W_I - W_Q\right)^2 = \left[\sqrt{C}\sin(m)T\right]^2$$

$$\sqrt{W_I^2 + W_Q^2} = \sqrt{C}\sin(m)T\sqrt{\left(1-\frac{2\theta}{\pi}\right)^2 + \left(\frac{2\theta}{\pi}\right)^2}$$

Substituting these expressions gives:

$$\sigma_\tau \approx \frac{\pi}{2\omega_t}\sqrt{\frac{N_0}{2}T}\frac{\sqrt{\left(1-2\frac{\omega_t\tau}{\pi}\right)^2 + \left(2\frac{\omega_t\tau}{\pi}\right)^2}}{\sqrt{C}\sin(m)T} =$$

$$= \frac{1}{4\sqrt{2}f_t}\frac{1}{\sqrt{\frac{P_{RC}}{N_0}T}}\sqrt{\left(1-2\frac{\omega_t\tau}{\pi}\right)^2 + \left(2\frac{\omega_t\tau}{\pi}\right)^2}$$

being $P_{RC} = C\sin^2(m)$ the ranging clock signal power.

Supposing that the 'coarse' value of the angle θ is evaluated by using first the discrimination for the quadrant (based on the sign of W_I and W_Q) and then its 'fine' value is evaluated in the range from 0 to π/2, in this case one has:

$$0 < 2\frac{\omega_t\tau}{\pi} < 1$$

Letting $x = 2\frac{\omega_t\tau}{\pi}$, it is observed that the function $f(x) = \sqrt{(1-x)^2 + (x)^2}$ assumes values in the range from $0.5\sqrt{2}$ to 1 for $0 \le x \le 1$ (or $0 \le \theta \le \frac{\pi}{2}$).

So it can written:

$$\sigma_\tau \le \frac{1}{4\sqrt{2}f_t}\frac{1}{\sqrt{\frac{P_{RC}}{N_0}T}}$$

$$\sigma_{Range} = c\cdot\frac{\sigma_\tau}{2} \le \frac{c}{8\sqrt{2}f_t}\frac{1}{\sqrt{\frac{P_{RC}}{N_0}T}}$$

The minimum value for $f(x)$ is for x=1/2 ($\theta = \omega_t \tau = \pi/4$); in this case it is $f(x) = 0.5\sqrt{2}$ and it can written:

$$\frac{c}{16 f_t} \frac{1}{\sqrt{\frac{P_{RC}}{N_0} T}} \leq \sigma_{Range} \leq \frac{c}{8\sqrt{2} f_t} \frac{1}{\sqrt{\frac{P_{RC}}{N_0} T}}$$

The ranging accuracy depends on the angle θ or on the delay τ to be measured. It is observed that one can achieve the best performances (smaller sigma value) in case the measurement is based on the following approach:

– preliminary estimation of the angle θ;

– rotation of the reference axes in order to have W_I and W_Q such that θ is around π/4;

– final accurate measurement.

In this case one can write:

$$\sigma_{Range\_OL\_sq\_sq} = \frac{c}{16 f_t} \frac{1}{\sqrt{\frac{P_{RC}}{N_0} T}} \qquad [m]$$

2.7.2.5 Comparison of Open- and Closed-Loop Performance

In order to minimize the spectral occupancy, the downlink ranging signal is on-board sine-wave shaped before transmission. For this reason the following two cases can be considered as the most common:

Chip Tracking Loop: $$\sigma_{Range\_CTL\_sine\_sq} = \frac{1}{\sqrt{2}} \frac{c}{8 f_{RC}} \cdot \sqrt{\frac{B_L}{(P_{RC}/N_0)}} \qquad [m]$$

Open Loop: $$\sigma_{Range\_OL\_sine\_sine} = \frac{c}{\sqrt{32\pi^2} f_{RC}} \cdot \sqrt{\frac{N_0}{P_{RC} T}} \qquad [m]$$

It can be seen in reference [6] that open and closed loop performances are the same if $2B_L = 1/T$.

Table 2-12 shows the effect of substituting in these expressions the same conditions indicated in the Blue Book (reference [1]):

- B_L=1 Hz (or T=0.5 s);
- Chip rate F_c = 2.068 Mchip/s; f_{RC}= F_c/2;
- P_R/N_0 =30 dBHz.

Table 2-12: Station Ranging Jitter Performances

Sequence	$\sigma_{Range\_CTL\_\sin\_sq}$	$\sigma_{Range\_OL\_\sin\_\sin}$
T4B	0.87 m	0.78 m
T2B	1.30 m	1.17 m

It is worth while to underline that these values consider only the downlink contribution or in other words they represent the overall end-to-end value just in case the on-board jitter contribution becomes negligible with respect to the downlink. For the overall end-to-end performances see 2.7.3.

2.7.3 END-TO-END PERFORMANCES

2.7.3.1 Introduction

In this subsection the general expression for the end-to-end ranging jitter is evaluated for the case of closed loop architecture with CTL implemented both on-board and at the Ground Station. It is found that the RSS approach for the end-to-end jitter is valid only in case the CTL loop bandwidth at the ground station is much wider than the one implemented on-board.

When the station loop bandwidth B_L is much narrower than the on-board bandwidth, a different expression must be applied. This might be the case when higher loop order and/or aided schemes are implemented at the ground station.

A similar expression is also derived for the case of Open Loop architecture at the ground station.

2.7.3.2 G/S Closed Loop Architecture

2.7.3.2.1 General

In case of '*sin_sq*' closed loop architecture implemented both for on-board and ground station (G/S), the variance for overall end-to-end ranging error in presence of thermal noise can be written as in reference [9] (see also 2.7.3.4):

$$\sigma^2_{Range} = \left(\frac{1}{\sqrt{2}}\frac{c}{8 f_{RC}}\right)^2 \left\{\frac{N_{01}}{2P_{RC1}}\left[\int_{-\infty}^{\infty}\left|H_1(f)H_2(f)\right|^2 df\right] + \frac{N_{02}}{2P_{RC2}}\left[\int_{-\infty}^{\infty}\left|H_2(f)\right|^2 df\right]\right\} \quad (\mathrm{m}^2)$$

In this expression is used also the equation derived for the CTL tracking jitter applying the same symbolism (f_{RC} = ranging clock frequency). The subscript 1 refers to the on-board CTL and the subscript 2 to the G/S CTL.

If the on-board and G/S CTL transfer function is known, the variance for overall end-to-end ranging error simply can be calculated by applying above equation with the evaluation of the two integrals. However, two approximations can be considered:

– G/S loop bandwidth $B_{L,2}$ much wider than on-board loop bandwidth $B_{L,1}$;

– G/S loop bandwidth $B_{L,2}$ much narrower than on-board loop bandwidth $B_{L,1}$.

These approximations allow representing and calculating the end-to-end ranging jitter in a simpler way.

2.7.3.2.2 G/S Loop Bandwidth Much Narrower Than On-Board Loop Bandwidth ($B_{L,1} << B_{L,2}$)

In this case (G/S loop bandwidth much wider than on-board loop bandwidth):

$$\sigma^2_{Range} \approx \left(\frac{1}{\sqrt{2}}\frac{c}{8 f_{RC}}\right)^2 \left\{\frac{N_{01}}{2P_{RC1}}\left[\int_{-\infty}^{\infty}\left|H_1(f)\right|^2 df\right] + \frac{N_{02}}{2P_{RC2}}\left[\int_{-\infty}^{\infty}\left|H_2(f)\right|^2 df\right]\right\} =$$

$$\approx \left(\frac{1}{\sqrt{2}}\frac{c}{8 f_{RC}}\right)^2 \left\{\frac{N_{01}}{P_{RC1}}\left[\frac{1}{2}\int_{-\infty}^{\infty}\left|H_1(f)\right|^2 df\right] + \frac{N_{02}}{P_{RC2}}\left[\frac{1}{2}\int_{-\infty}^{\infty}\left|H_2(f)\right|^2 df\right]\right\} =$$

$$= \left(\frac{1}{\sqrt{2}}\frac{c}{8 f_{RC}}\right)^2 \left\{\frac{N_{01}}{P_{RC1}} B_{L,1} + \frac{N_{02}}{P_{RC2}} B_{L,2}\right\} \quad (\mathrm{m}^2)$$

$$\sigma_{Range} \approx \sqrt{\left[\sigma_{Range\_CTL\_\sin\_sq\_1}\right]^2 + \left[\sigma_{Range\_CTL\_\sin\_sq\_2}\right]^2} \quad (\mathrm{m})$$

The condition $B_{L,1} << B_{L,2}$ leads to a worst case condition, with the rms ranging error as the RSS of the uplink and downlink contribution calculated separately. However, in this particular case (with $B_{L,1} << B_{L,2}$), these measurements can be further processed (averaged) in order to reduce the rms error due to the thermal noise.

2.7.3.2.3 G/S Loop Bandwidth Much Wider Than On-Board Loop Bandwidth ($B_{L,1} >> B_{L,2}$)

In this case (G/S loop bandwidth much narrower than on-board loop bandwidth):

$$\sigma^2_{Range} \approx \left(\frac{1}{\sqrt{2}}\frac{c}{8 f_{RC}}\right)^2 \left\{\frac{N_{01}}{2P_{RC1}}\left[\int_{-\infty}^{\infty}|H_2(f)|^2 df\right] + \frac{N_{02}}{2P_{RC2}}\left[\int_{-\infty}^{\infty}|H_2(f)|^2 df\right]\right\} =$$

$$= \left(\frac{1}{\sqrt{2}}\frac{c}{8 f_{RC}}\right)^2 \left[\frac{1}{2}\int_{-\infty}^{\infty}|H_2(f)|^2 df\right]\left\{\frac{N_{01}}{P_{RC1}} + \frac{N_{02}}{P_{RC2}}\right\} \quad (\text{m}^2)$$

$$\sigma_{Range} = \frac{1}{\sqrt{2}}\frac{c}{8 f_{RC}}\sqrt{B_{L,2}\left\{\frac{N_{01}}{P_{RC1}} + \frac{N_{02}}{P_{RC2}}\right\}} \quad (\text{m})$$

This loop must be able to track the received ranging clock affected by the thermal downlink noise but also by the on-board tracking jitter transmitted (to the G/S) on the regenerated PN ranging signal. So the G/S loop (and also its bandwidth B_{L2}) must be dimensioned considering also the on-board tracking performances.

2.7.3.3 G/S Open Loop Architecture

It is not so immediate to calculate the correct expression for this case; however, for the open loop can easily be applied the approximation $B_{L,1} >> 1/T$ (where $B_{L,1}$ is the on-board CTL bandwidth and T is the G/S integration time). Using the same approach applied in 2.7.3.2.3 and considering the jitter expression for the open loop '*sine_sine*' case one can write:

$$\sigma_{Range} \approx \frac{c}{\sqrt{32\pi^2}\, f_{RC}}\sqrt{\frac{1}{T}\left[\frac{N_{01}}{P_{RC1}} + \frac{N_{02}}{P_{RC2}}\right]} \quad (\text{m})$$

The advantage of the Open Loop architecture is that no tracking loop is needed on the ranging clock for the delay estimation, so the integration time T is not constrained by the on-board tracking jitter values. However, it should be noted that the Open Loop architecture requires coherency between the chip rate and the carrier frequency.

2.7.3.4 End-to-End Analysis

The end-to-end ranging is implemented through the following functions (a CTL for on-board and G/S is assumed):

– Uplink Ground Station (G/S for short)

  • generation of the uplink ranging signal;

  • PM modulation of uplink carrier with the ranging signal.

– On-Board

  • carrier demodulation;

  • ranging signal acquisition and tracking (based on a CTL architecture);

  • coherent ranging signal generation (phase synchronized with the uplink recovered ranging clock and phase);

  • PM modulation of the downlink carrier with the regenerated ranging signal.

– Downlink G/S

  • carrier demodulation;

  • G/S ranging signal acquisition and tracking based on the CTL;

  • comparison between the received and transmitted code phase for delay measurement.

In the following analysis, for simplicity, the carrier modulation and demodulation process as an ideal process is considered. In addition focus is on the ranging clock recovery, this is the component (of the ranging signal) used for accurate ranging measurement. This is equivalent to consider what is defined as the '*Equivalent Baseband Model*' represented by the block diagram in figure 2-19, where the linear PLL theory has been applied.

In addition instead of the CTL, a classical PLL is considered (assuming the PN ranging based on the ranging clock only). The extension of the analysis results to the CTL case can be easily applied as final step with the introduction of the proper multiplication coefficients (related to the CTL architecture) and taking into account also the speed of light for the indication of the rms error in meter.

In this way it can be written for the on-board CTL:

$G_1(s) = K_{d1}F_1(s)\dfrac{K_{V1}}{s}$ is the open loop transfer function of the on-board CTL;

K_{d1} is the phase detector gain of the on-board CTL;

K_{V1} is the VCO or NCO constant of the on-board CTL;

$H_1(s) = \frac{G_1(s)}{1+G_1(s)}$ is the closed loop transfer function;

P_{RC1} is the on-board ranging clock power at CTL input;

$\frac{P_{RC1}}{N_{01}}$ is the on-board ranging clock power over noise spectral density at CTL input.

While for the G/S CTL:

$G_2(s) = K_{d2}F_2(s)\frac{K_{V2}}{s}$ is the open loop transfer function of the G/S CTL;

K_{d2} is the phase detector gain of the G/S CTL;

K_{V2} is the VCO or NCO constant of the G/S CTL;

$H_2(s) = \frac{G_2(s)}{1+G_2(s)}$ is the closed loop transfer function;

P_{RC2} is the G/S ranging clock power at CTL input;

$\frac{P_{RC2}}{N_{02}}$ is the G/S ranging clock power over noise spectral density at CTL input.

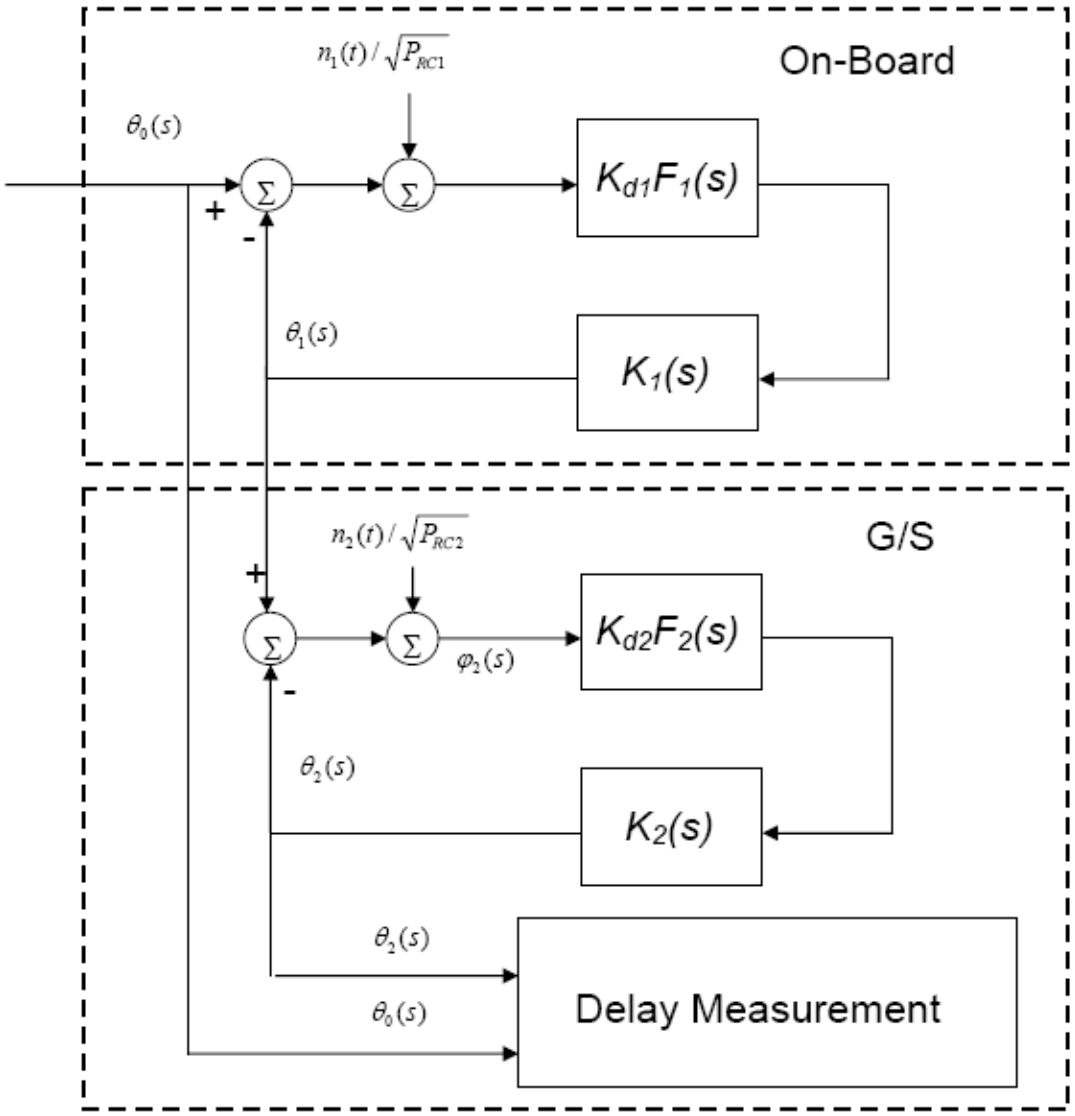

Figure 2-19: 'Equivalent Baseband Model' for End-to-End Ranging Measurement

For the thermal noise is assumed (in both cases at the CTL input) the AWGN model with 2-sided power spectral density $N_{01}/2$ for on-board and $N_{02}/2$ for on ground. Applying Heaviside's notation, the on-board estimate of the uplink ranging clock phase is written:

$$\theta_1(s) = H_1(s)\theta_o(s) + \frac{N_1(s)}{\sqrt{P_{RC1}}} H_1(s)$$

It should be noted that:

– $N_1(s)$ is the Laplace transform of a test signal $n_1(t)$ necessary to evaluate the transfer function; later on $n_1(t)$ will represent the noise random process related to the on-board AWGN model with power spectral density $N_{01}/2$;

– $\theta_1(s)$ is also the phase of the on-board transmitted ranging clock.

In the same way one can write the estimate of the ranging clock phase at the ground station:[14]

$$\theta_2(s) = H_2(s)\theta_1(s) + \frac{N_2(s)}{\sqrt{P_{RC2}}} H_2(s)$$

where $N_2(s)$ is the equivalent of $N_1(s)$ at the station (in this case the power spectral density is $N_{02}/2$.) One can write the estimate of the ranging clock phase θ_2 at the ground station as a function of the ranging clock phase θ_0 as transmitted by the ground station:

$$\theta_2(s) = H_1(s)H_2(s)\theta_0(s) + H_1(s)H_2(s)\frac{N_1(s)}{\sqrt{P_{RC1}}} + H_2(s)\frac{N_2(s)}{\sqrt{P_{RC2}}}$$

Where the first term $[H_1(s)H_2(s)\theta_0(s)]$ represents the system deterministic response, while the last two terms are relevant to the system random response.

For the variance of the error in the estimation of the phase θ_0 one can write:

$$\sigma^2 = \frac{1}{2\pi}\frac{N_{01}}{2P_{RC1}}\left[\int_{-\infty}^{\infty}\left|H_1(\omega)H_2(\omega)\right|^2 d\omega\right] + \frac{1}{2\pi}\frac{N_{02}}{2P_{RC2}}\left[\int_{-\infty}^{\infty}\left|H_2(\omega)\right|^2 d\omega\right] \ (rad^2)$$

Using the following definitions:

System Noise Equivalent Bandwidth: $B_{L,eq} = \frac{1}{2}\frac{1}{2\pi}\int_{-\infty}^{\infty}\left|H_1(\omega)H_2(\omega)\right|^2 d\omega$

On-board CTL Noise Equivalent Bandwidth: $B_{L,1} = \frac{1}{2}\frac{1}{2\pi}\int_{-\infty}^{\infty}\left|H_1(\omega)\right|^2 d\omega$

G/S Noise CTL Equivalent Bandwidth: $B_{L,2} = \frac{1}{2}\frac{1}{2\pi}\int_{-\infty}^{\infty}\left|H_2(\omega)\right|^2 d\omega$

one can write for the variance of the error:

[14] Neglected in this analysis is the phase delay relevant to the RF path (media) between the G/S and the S/C together with other delay contributions due to on-board and on-ground electronics. However this is not relevant for the jitter evaluation.

$$\sigma^2 = \frac{N_{01}}{P_{RC1}} B_{L,eq} + \frac{N_{02}}{P_{RC2}} B_{L,2} \quad (rad^2)$$

As indicated in 2.7.2.2 for the '*sin_sq*' case the CTL performances in terms of ranging rms error are represented by the following expression:

$$\sigma_{Range\_CTL\_\sin\_sq} = \left(\frac{1}{\sqrt{2}} \frac{c}{8 f_{RC}} \right) \cdot \sqrt{\frac{B_L}{(P_{RC}/N_0)}} \qquad \text{(m)}$$

So for the overall end-to-end ranging rms error one can write:

$$\sigma_{Range} = \left(\frac{1}{\sqrt{2}} \frac{c}{8 f_{RC}} \right) \left\{ \frac{1}{2\pi} \frac{N_{01}}{2P_{RC1}} \left[\int_{-\infty}^{\infty} |H_1(\omega) H_2(\omega)|^2 \, d\omega \right] + \frac{1}{2\pi} \frac{N_{02}}{2P_{RC2}} \left[\int_{-\infty}^{\infty} |H_2(\omega)|^2 \, d\omega \right] \right\}^{\frac{1}{2}} \quad \text{(m)}$$

In all the equations above indicated the following units are used:

– the frequency (i.e., f_{RC}) in Hz;

– the signal power (i.e., P_{RC}) in Watt;

– the noise power spectral density (i.e., N_{01} and N_{02}) in Watt/Hz.

2.8 INTERFERENCE WITH TELEMETRY AND TELECOMMAND

2.8.1 INTRODUCTION

The possibility of mutual interference between telecommand and ranging, and between telemetry and ranging when the signals are transmitted simultaneously on the same carrier has been analyzed and simulated. Because of the large range of possible bit rates and chip rates, it was not viable to consider all possible cases. Instead, some best (minimal spectral overlap) and worst (maximum spectral overlap) cases were considered.

2.8.2 UPLINK TC AND RANGING COMPATIBILITY

Telecommand transmission in accordance with recommendations 2.2.4 and 2.2.7 of CCSDS 401.0-B (reference [14]) can in principle be performed at the same time of ranging.

The worst case of recommendation 2.2.4 of CCSDS 401.0-B vis-à-vis ranging consists in the telecommand bits BPSK phase modulating a 16 kHz subcarrier with a maximum data rate of 4 kbps, the composite resulting signal phase modulating a residual carrier. Obviously, the spectral overlap between such telecommand signal and the PN ranging signal is minimal for chip rates higher than 250 kchip/s. Simulations (see reference [10]) performed in these cases have shown that the mutual ranging and telecommand losses are negligible independently from ranging code and shaping waveform. On the other hand, in case a chip rate around 32

kchip/s is used, the resulting clock at 16 kHz would severely interfere with the 16 kHz telecommand subcarrier and should not be transmitted at the same time.

The signal transmitted in the uplink is (see figure 2-20):

$$x_u(t) = A_c \cos[2\pi f_u t + m_{RG} x_{RG}(t) + m_{TC} x_{TC}(t)]$$

where

– f_u is the uplink center frequency

– m_{RG} is the phase modulation index for the ranging signal;

– m_{TC} is the phase modulation index for the telecommand signal;

– $x_{RG}(t)$ is the ranging signal:

$$x_{RG}(t) = \sum_{k=-\infty}^{\infty} c_k h(t - kT_c)$$

and $h(t)$ is different from zero only for $t \in [0, T_c]$, and may be either a rectangular pulse ($h(t) = h_{sq}(t)$) or a half cycle sine ($h(t) = h_{sin}(t) = \sin(\pi t/T_c)$), $T_c = 1/R_c$ is the chip interval and R_c is the chip rate (2 Mchip/s in the simulations), $c_k = \pm 1$ is the periodic sequence of values determined by the chosen ranging code;

– $x_{TC}(t)$ is the telecommand signal:

$$x_{TC}(t) = \sum_{k=-\infty}^{\infty} d_k g_{TC}(t - kT_{TC})$$

and $g_{TC}(t) = \sin(2\pi f_s t)$ for $t \in [0, T_{TC}]$, and zero elsewhere, $T_{TC} = 1/R_{TC}$ is the telecommand bit interval and R_{TC} is the bit rate for the telecommand data ($R_{TC} = 4$ kbit/s and $f_s = 16$ kHz in the simulations), $d_k = \pm 1$ is a random sequence.

If the rectangular pulse $h_{sq}(t)$ is used for the ranging signal, then the energy used to transmit one ranging chip and one telecommand bit are, respectively

$$E_{RG,u} = \tfrac{1}{2} A_c^2 J_0^2(m_{TC}) \sin^2(m_{RG}) T_c;\ E_{TC,u} = A_c^2 J_1^2(m_{TC}) \cos^2(m_{RG}) T_{TC};$$

if the sinusoidal pulse $h_{\sin}(t)$ is used, then

$$E_{RG,u} = A_c^2 J_0^2(m_{TC}) J_1^2(m_{RG}) T_c;\ E_{TC,u} = A_c^2 J_1^2(m_{TC}) J_0^2(m_{RG}) T_{TC}.$$

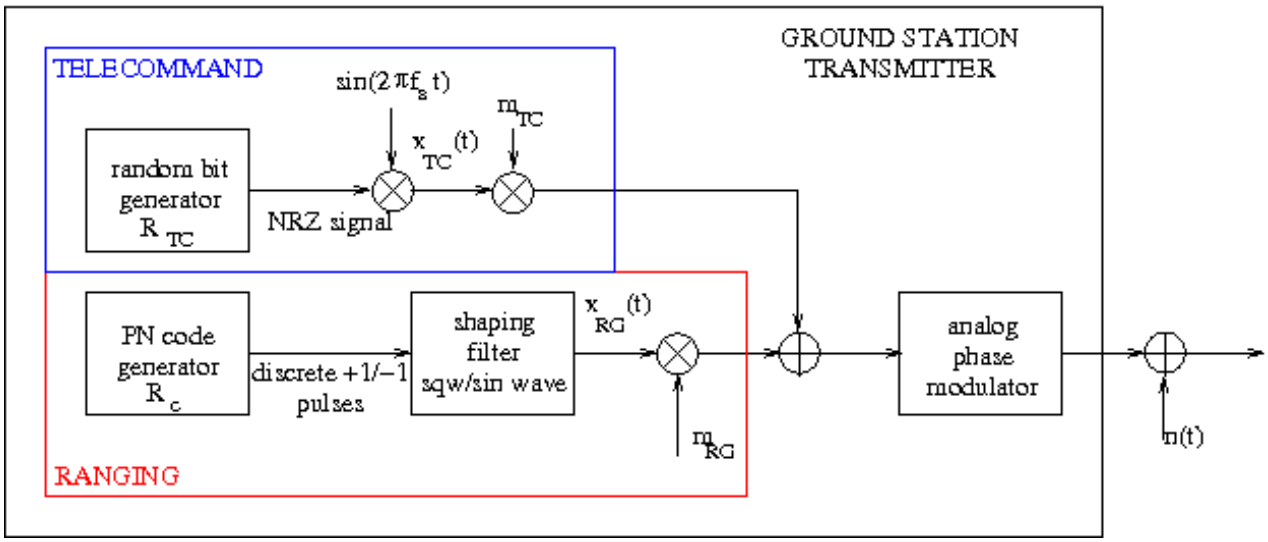

Figure 2-20: G/S Transmitter Structure

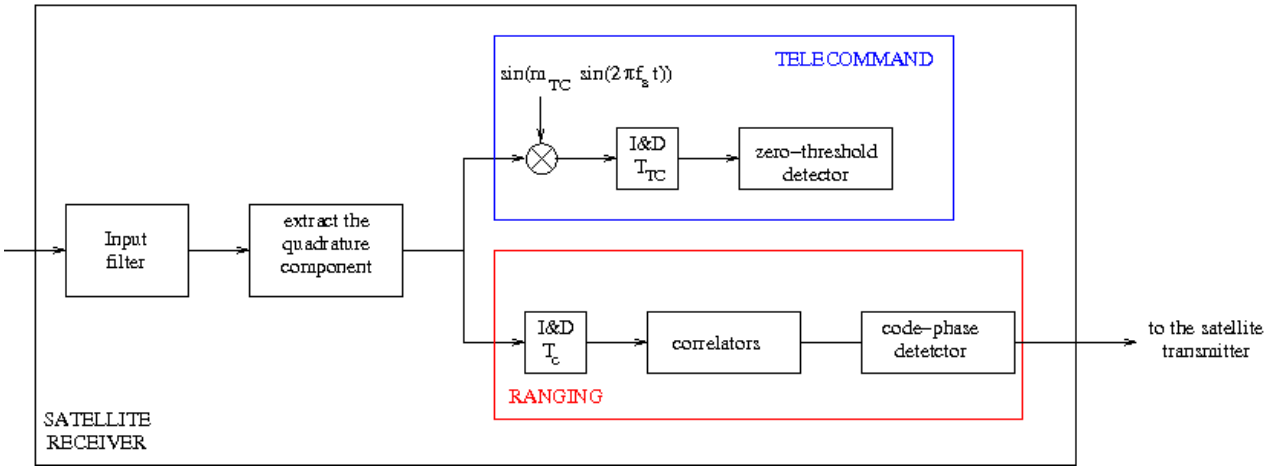

Figure 2-21: S/C Receiver Structure

The satellite receiver structure is shown in figure 2-21; it is the optimum receiver for the telecommand system and for the ranging system with pulse $h_{sq}(t)$, while, because of the presence of a simple integrate and dump filter, it is not optimum for the ranging system with $h_{\sin}(t)$.

If the ranging signal is absent, then the error probability for the telecommand bit is

$$P_{id,TC}(e) = \frac{1}{2}\, erfc\, \sqrt{\frac{E_{TC,u}}{N_0}}.$$

If the ranging signal is present, then the telecommand system suffers from a small loss (see figure 2-22) and $P_{TC}(e) > P_{id,TC}(e)$. Table 2-13 lists the measured loss for $P_{TC}(e) = 10^{-4}$, $m_{RG} = 0.7$ rad and $m_{TC} = 1.0$ rad. The losses shown here and in 2.8.3 were all measured through simulation.

Table 2-13: Uplink Losses for the TC System at $P_{TC}(e)=10^{-4}$, $m_{TC}=1$ rad, $m_{RG}=0.7$ rad

code	$h(t) = h_{sq}(t)$	$h(t) = h_{sin}(t)$
T2B	0.04 dB	0.06 dB
T4B	0.02 dB	0.05 dB

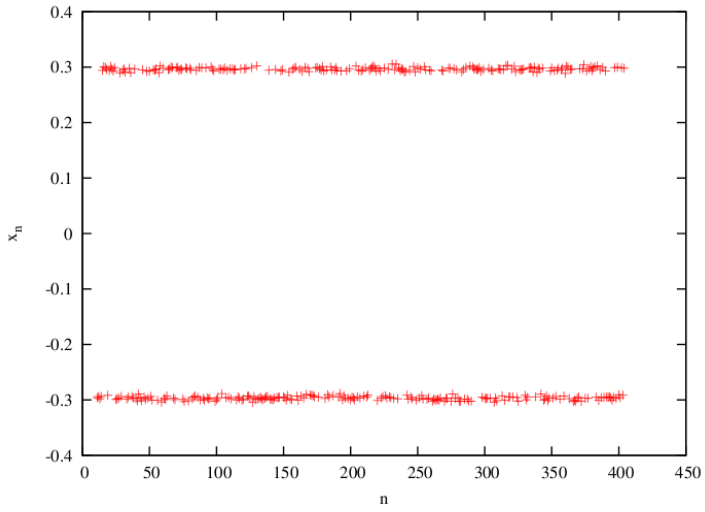

Figure 2-22: Input of the TC Zero-Threshold Detector in the Presence of Ranging Interference (No Noise), $m_{TC}=1$ rad, $m_{RG}=0.7$rad

As for the ranging system, the case with $h_{\sin}(t)$ suffers from a loss equal to

$$L_{\sin} = 10\log_{10}\frac{2J_1^2(m_{RG})}{E_0^2(m_{RG})}, \quad E_0(x) = \frac{1}{\pi}\int_0^{\pi}\sin(x\sin(u))du$$

because of the pulse mismatch in the integrate & dump receiver; this loss amounts to 0.85 dB when m_{RG}=0.7 rad. Moreover, there is a further loss resulting from the interfering telecommand signal. Table 2-14 lists the losses for the ranging system at $P_{RNG}(e)=10^{-6}$ (i.e., probability that the PN code phase is wrongly estimated), with $m_{TC}=1$ *rad*, $m_{RG}=0.7$. The

losses practically do not depend on the target error probability and the system with $h_{\sin}(t)$ shows an overall loss L_{sin} which is slightly larger than 0.85 dB+ L_{sq}.

Table 2-14: Uplink Losses L_{sq} (Left) L_{sin} (Right) for the RNG System at $P_{RNG}(e)=10^{-6}$, m_{TC}=1 rad, m_{RG}=0.7 rad

code	$h(t) = h_{sq}(t)$	$h(t) = h_{sin}(t)$
T2B	0.19 dB	1.07 dB
T4B	0.19 dB	1.07 dB

Therefore, the loss due to telecommand interference alone is of the order of 0.2 dB.

The modulation scheme of recommendation 2.2.7 of CCSDS 401.0-B consists in directly bi-phase modulating the residual carrier with data rates as high as 256 kbps. Given that such scheme is normally used for telemetry transmission, the mutual interference with ranging is only evaluated in 2.8.3. However, the results obtained there for telemetry are applicable to telecommand as well.

2.8.3 DOWNLINK TM AND RANGING COMPATIBILITY

2.8.3.1 General

The transmitted signal in the downlink is (see figure 2-23):

$$x_d(t) = A_c \cos[2\pi f_d t + m_{RG} x_{RG}(t) + m_{TM} x_{TM}(t)]$$

where

- f_d is the downlink center frequency;
- m_{RG} is the phase modulation index for the ranging signal;
- m_{TM} is the phase modulation index for the telemetry signal ($m_{TM} = 1.25$ rad in the simulations);
- $x_{RG}(t)$ is the ranging signal:

$$x_{RG}(t) = \sum_{k=-\infty}^{\infty} c_k h(t - kT_c)$$

and $h(t) = h_{sq}(t)$ or $h(t) = h_{sin}(t)$ as for the uplink;

– $x_{TM}(t)$ is the telemetry signal:

$$x_{TM}(t) = \sum_{k=-\infty}^{\infty} d_k \, p_{TM}(t - kT_{TM})$$

and $p_{TM}(t) = 1$ for $t \in [0, T_{TM}/2]$, $p_{TM}(t) = -1$ for $t \in [T_{TM}/2, T_{TM}]$, $T_{TM} = 1/R_{TM}$ is the telemetry symbol interval and R_{TM} is the symbol rate for the telemetry data (R_{TM} = 500 ks/s in the simulations), $d_k = \pm 1$ is a random sequence.

If the rectangular pulse $h_{sq}(t)$ is used for the ranging signal, then the energies used to transmit one ranging chip and one telemetry symbol are, respectively:

$$E_{RG,d} = \frac{A_c^2}{2}\cos^2[m_{TM}]\sin^2[m_{RG}]T_c; \; E_{TM,d} = \frac{A_c^2}{2}\cos^2[m_{RG}]\sin^2[m_{TM}]T_{TM}$$

while they are

$$E_{RG,d} = \frac{A_c^2}{2}\cos^2[m_{TM}]2J_1^2(2m_{RG})T_c; \; E_{TM,d} = \frac{A_c^2}{2}J_0^2(m_{RG})\sin^2[m_{TM}]T_{TM}$$

if the sinusoidal pulse $h_{\sin}(t)$ is used. The G/S receiver is shown in figure 2-24 for a transmitted pulse $h_{sq}(t)$, and in figure 2-25 for a transmitted pulse $h_{\sin}(t)$ (at the ground station a more complex receiver is feasible).

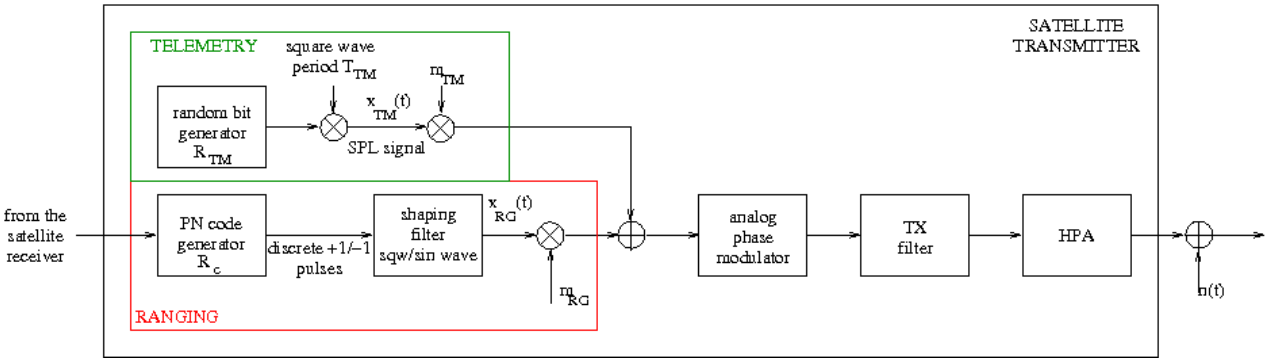

Figure 2-23: S/C Transmitter Structure

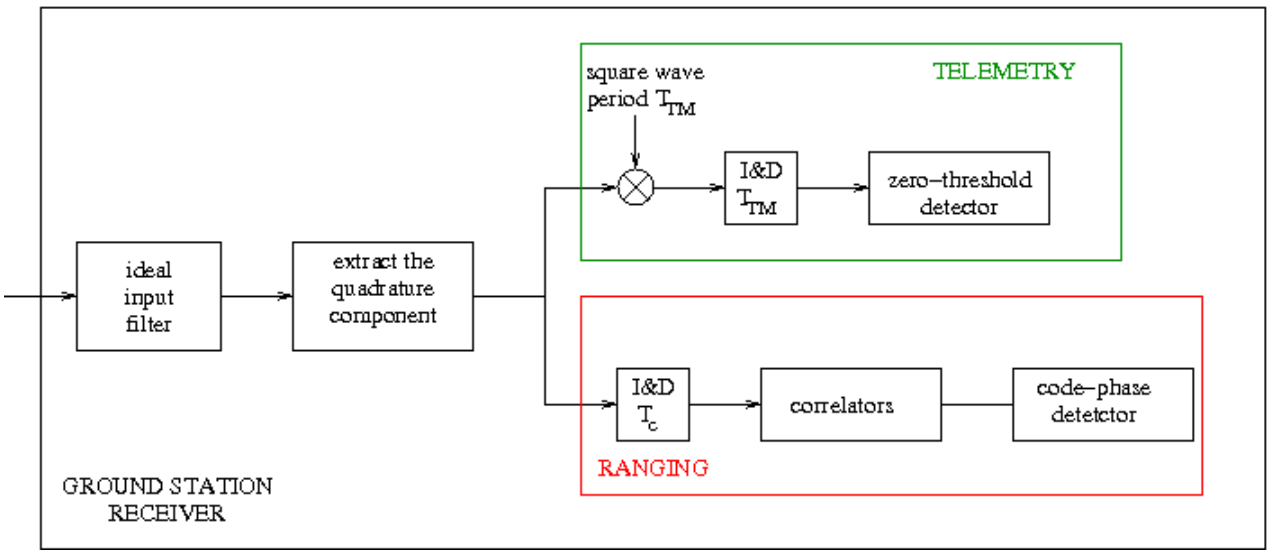

Figure 2-24: G/S Receiver Structure for Pulse $h_{sq}(t)$

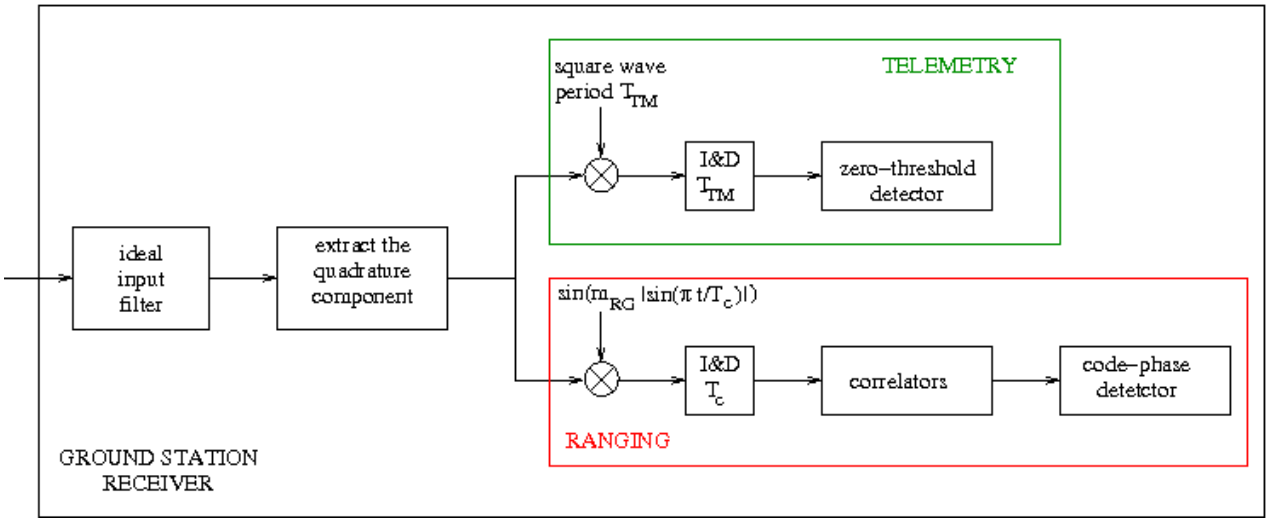

Figure 2-25: G/S Receiver Structure for Pulse $h_{\sin}(t)$

2.8.3.2 CTL Tracking Jitter

The quadrature component of the noiseless received signal, used for the detection of telemetry bits and ranging chips and chip clock synchronization is:

$$x_q(t) = A_c \sin[m_{RG} x_{RG}(t)] \cos[m_{TM} x_{TM}(t)]$$

$$+ A_c \cos[m_{RG} x_{RG}(t)] \sin[m_{TM} x_{TM}(t)]$$

and, for $h(t) = h_{sq}(t)$ (the only case analyzed in this subsection):

$$x_q(t) = A_c \cos[m_{TM}]\sin[m_{RG}]\sum_{k=-\infty}^{\infty} c_k h_{sq}(t - kT_c)$$

$$+ A_c \cos[m_{RG}]\sin[m_{TM}]\sum_{k=-\infty}^{\infty} d_k p_{TM}(t - kT_{TM})$$

$$= x_{q,RG}(t) + x_{q,TM}(t).$$

Since the ranging signal and the telemetry signal are statistically independent the power spectrum of $x_q(t)$ is simply:

$$G_{x_q}(f) = (A_c \cos[m_{TM}]\sin[m_{RG}])^2 G_{RG}(f) + (A_c \cos[m_{RG}]\sin[m_{TM}])^2 G_{TM}(f),$$

where

$$G_{TM}(f) = T_{TM}\left[\frac{\sin^2(\pi f T_{TM}/2)}{\pi f T_{TM}/2}\right]^2$$

is the power spectrum of $\sum_{k=-\infty}^{\infty} d_k p_{TM}(t - kT_{TM})$;

$$G_{RG}(f) = \sum_{k=-\infty}^{\infty} |\nu_k|^2 \, \delta(f - k/T_r)$$

is the power spectrum of the periodic ranging signal $\sum_{k=-\infty}^{\infty} c_k h_{sq}(t - kT_c)$ (period $T_r = L_r T_c$), being

$$|\nu_n|^2 = |C(n)|^2 \left[\frac{\sin(\pi n/L_r)}{\pi n/L_r}\right]^2, \text{ with } C(n) = \frac{1}{L_r}\sum_{k=0}^{L_r-1} c_k e^{-j2\pi nk/L_r}.$$

As far as the chip clock synchronization is concerned, of interest is the power spectrum at frequency $f_{RC} = 1/(2T_c) = R_c/2 = (L_r/2)/T_r$. At this frequency, $G_{RG}(f)$ includes a spectral line with coefficient

$$|\nu_{L_r/2}|^2 = |C(L_r/2)|^2 \left[\frac{2}{\pi}\right]^2$$

and $|C(L_r/2)|^2$ is given in table 2-15 for the considered ranging codes (see also table 2-3).

Table 2-15: Coefficient $C(L_r/2)$ for Codes T2B and T4B

code	$C(L_r/2)$	$10\log_{10}\lvert C(L_r/2)\rvert^2$
T2B	-0.62736	-4.05 dB
T4B	-0.9368	-0.55 dB

The power spectrum continuous component $G_{TM}(f)$ at f_{RC} is equal to

$$G_{TM}(1/(2T_c)) = T_{TM}\left[\frac{\sin^2(\pi T_{TM}/(4T_c))}{\pi T_{TM}/(4T_c)}\right]^2$$

Therefore, as far as the chip synchronization is concerned, the ratio between the useful component of the ranging signal and the interference component of the telemetry signal in a bandwidth B_L is

$$\eta = \left[\frac{\tan(m_{RG})}{\tan(m_{TM})}\right]^2 |C(L_r/2)|^2 \left[\frac{2}{\pi}\right]^2 \frac{[\pi R_c/(4R_{TM})]^2}{T_{TM} B_L [\sin^2(\pi R_c/(4R_{TM}))]^2}$$

Of course, the higher is η, the better is the CTL performance. It is seen that η depends on the ratio $R_c/(4R_{TM})$: if $R_c = 2$ Mchip/s and $R_{TM} = 500$ kbit/s, then $R_c/(4R_{TM}) = 1$ and $\eta \to \infty$; for other values of R_c there are finite values of η. The system was therefore analyzed for $R_c = 2$ Mchip/s and $R_c = 1.9$ Mchip/s. Figure 2-26 shows the CTL transient in the simpler case in which only the clock component of the ranging signal is generated (so that the CTL is the optimum synchronizer and $C(L_r/2)=1$); the effects of the telemetry signal can be seen as a mean offset with respect to the ideal synchronization time (which corresponds to a mean error in the estimation of the distance, i.e., lack of accuracy), but the offset is present only when the CTL bandwidth is very large. Therefore telemetry interference on the ranging chip synchronization is present, but it can be considered negligible for normal loop bandwidths.

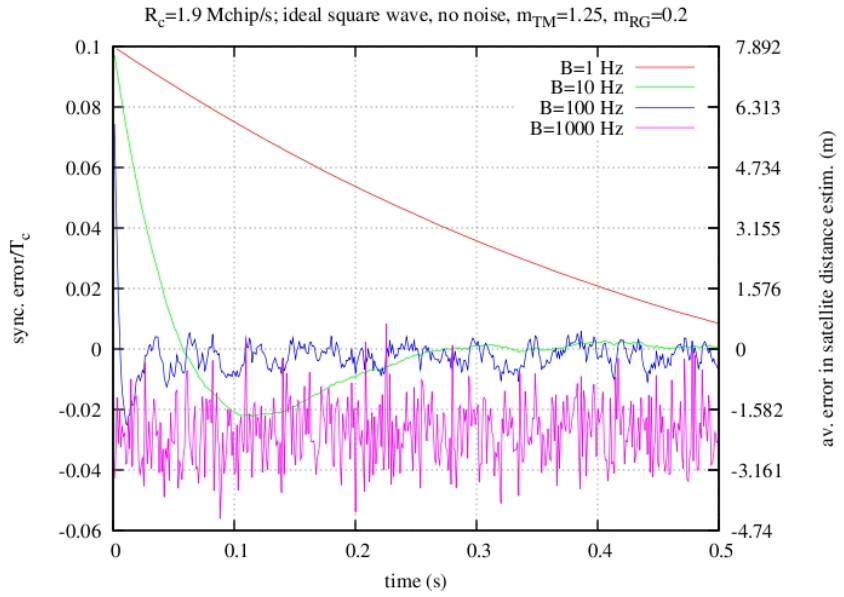

Figure 2-26: CTL Acquisition Transient, Only Clock Component for the Ranging Signal, m_{TM}=1.25 rad, m_{RG}=0.2 rad, R_{TM}=500 ks/s, R_c=1.9Mc/s

As for the CTL timing jitter (i.e., estimation precision), figures 2-27 and 2-28 show the measured normalized variance $\sigma_\varepsilon^2 / T_c^2$ for chip rates 2 Mc/s and 1.9 Mc/s. The curve labelled 'ideal baseband' is related to the case in which the CTL has an input equal to the clock component plus noise at baseband (no telemetry), so that $\sigma_\varepsilon^2 / T_c^2 = B_L /(4P_r / N_0) = B_L T_c /(4E_c / N_0)$ (as obtained in 2.5.1). The other curves are related to the PN ranging codes T2B and T4B interfered by the telemetry signals: the theoretical ranging variance in the absence of telemetry interference is

$$\sigma_\varepsilon^2 / T_c^2 = B_L /(4P_r / N_0) = B_L T_c /(4 |C(L_r / 2)|^2 \; E_{RG,d} / N_0)$$

and therefore a given ranging variance is obtained with a ratio $E_{RG,d} / N_0$ which is 0.55 or 4.05 dB higher than in the ideal case for codes T4B and T2B, respectively. The curves shown in the figures for codes T2B and T4B are shifted by 0.55 and 4.05 dB when the variance is around 10^{-3}, while the shift becomes slightly larger for smaller variances (further loss of about 0.5 dB at 10^{-5}). The extra loss is equal for the two codes. In conclusion, telemetry has a negligible effect on the CTL precision and accuracy.

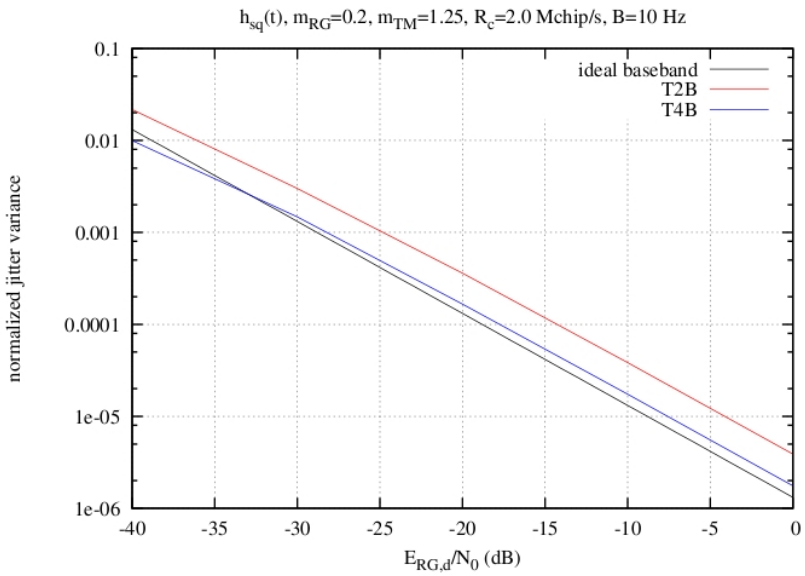

Figure 2-27: Normalized CTL Timing Ranging Variance for the Case $h_{sq}(t)$, m_{TM}=1.25 rad, m_{RG}=0.2 rad, R_{TM}=500 ks/s, R_c=2Mc/s

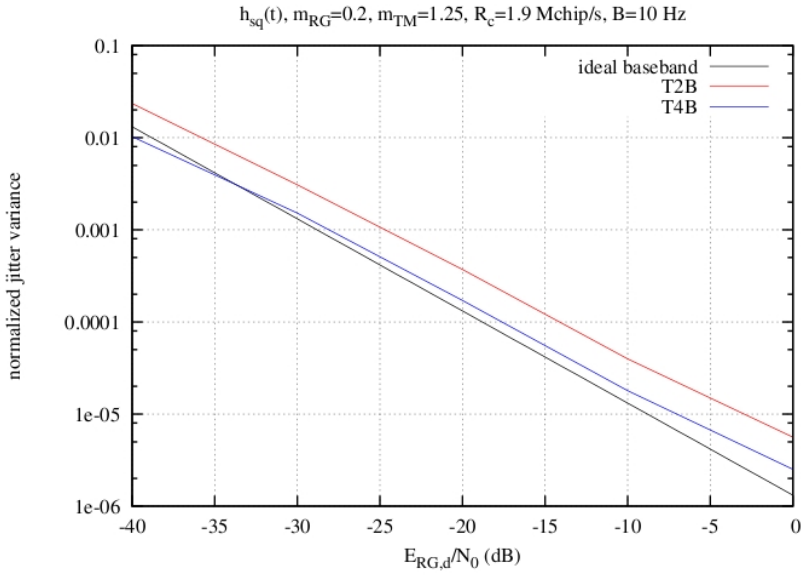

Figure 2-28: CTL Ranging Variance for the Case $h_{sq}(t)$, m_{TM}=1.25 rad, m_{RG}=0.2 rad, R_{TM}=500 ks/s, R_c=1.9Mc/s

2.8.3.3 PN Ranging Acquisition

As for the ranging system, the losses due to the interfering telemetry signal were measured through simulation, and they are given in table 2-16 for the case m_{TM}=1.25 rad, m_{RG}=0.7 rad: code T4B suffers from higher losses and pulse $h_{sq}(t)$ is more robust against the interference. Figure 2-29 shows the ranging losses due to the telemetry signal as function of m_{RG}, when m_{TM}=1.25 rad and $R_c = 2$ Mchip/s, $R_{TM} = 500$ kbit/s: the loss decreases with m_{RG}, and the best case is that with code T2B and $h_{sq}(t)$. Smaller losses result if telemetry and ranging are not synchronous as is normally the case.

Table 2-16: Downlink Losses L_{sq} (Left) L_{sin} (Right) for the RNG System at $P_{RG}(e)=10^{-6}$, m_{TM}=1.25 rad, m_{RG}=0.7

code	$h(t) = h_{sq}(t)$	$h(t) = h_{sin}(t)$
T2B	0.06 dB	0.10 dB
T4B	0.63 dB	1.16 dB

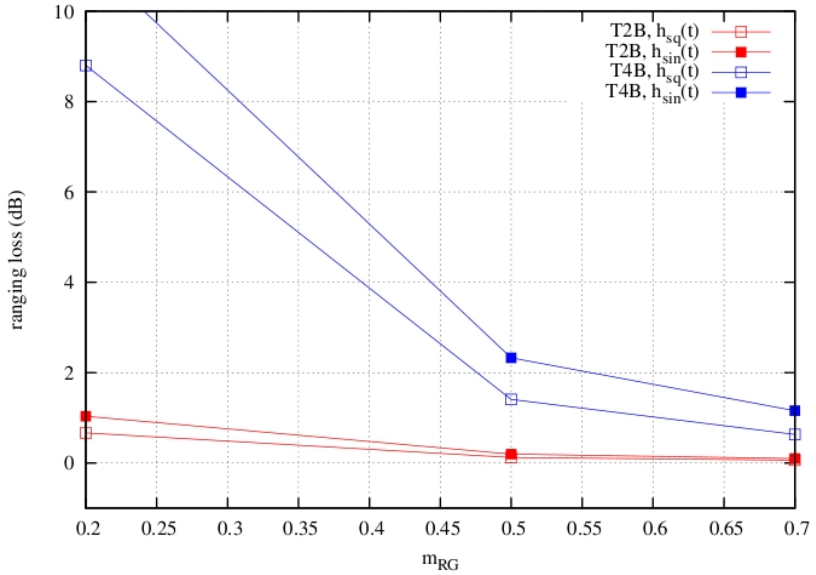

Figure 2-29: Downlink Ranging Losses (dB) with Respect to m_{RG}, for m_{TM}=1.25 rad

2.8.3.4 TM BER

In the absence of ranging, the telemetry symbol error probability is

$$P_{id,TM}(e) = \frac{1}{2}\, erfc\, \sqrt{\frac{E_{TM,d}}{N_0}}\ .$$

Ranging introduces interference, as shown in figure 2-30: in the absence of noise and ranging, the detector input only takes the two values ±0.7, while in the presence of ranging 4 levels appear, and the lowest level in absolute value (i.e., 0.5) is more frequent for code T2B (left) than T4B (right). Table 2-17 lists the losses of the telemetry system at $P_{TM}(e)=10^{-4}$, $m_{TM}=1.25$ rad, $m_{RG}=0.7$, and it is possible to observe that code T4B generates a smaller loss, and that pulse $h_{\sin}(t)$ produces less interference than pulse $h_{sq}(t)$. Figure 2-31 shows the telemetry losses due to the ranging signal as function of m_{RG}, when $m_{TM}=1.25$ rad: the loss increases with m_{RG}, and the best case is that with code T4B and $h_{\sin}(t)$. Further simulations were run in order to measure the losses when a non-integer ratio exists between the chip rate and the TM symbol rate; figure 2-32 shows the cases of $R_{TM}=500$ ks/s and $R_c=1.7$ Mc/s or 1.9 Mc/s: the differences between the cases $h_{\sin}(t)$ and $h_{sq}(t)$ is much reduced, and pulse $h_{sq}(t)$ is now to be preferred, while code T2B again introduces a higher loss on the telemetry system than code T4B. In conclusion, the ranging signal worsens the telemetry system performance and code T2B has a greater impact than code T4B; the measured losses are below 1 dB, but the exact loss depends on the chosen parameters.

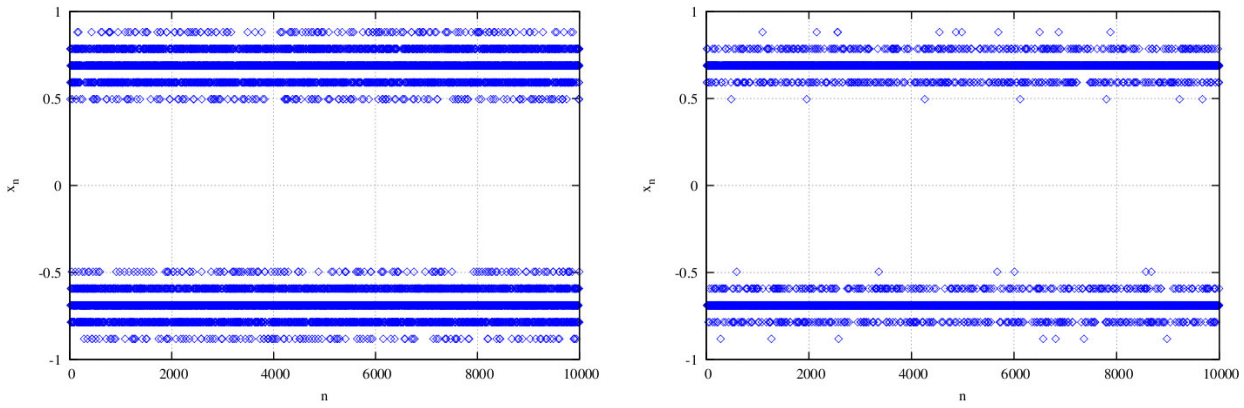

Figure 2-30: Samples at the Input of the Zero-Threshold Detector of the Telemetry Receiver; Case of Pulse $h_{sq}(t)$, $m_{TM}=1.25$ rad, $m_{RG}=0.7$ rad, Codes T2B (Left) and T4B (Right), No Noise

Table 2-17: Downlink Losses for the TM System at $P_{TM}(e)=10^{-4}$, $m_{TM}=1.25$ rad, $m_{RG}=0.7$

code	$h(t) = h_{sq}(t)$	$h(t) = h_{sin}(t)$
T2B	0.84 dB	0.29 dB
T4B	0.18 dB	0.09 dB

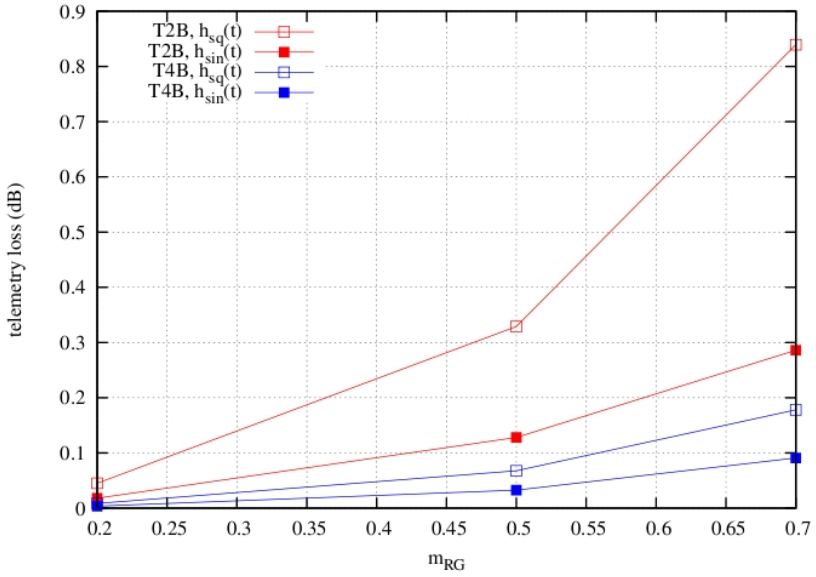

Figure 2-31: Downlink Telemetry Losses (dB) with Respect to m_{RG}, for $m_{TM}=1.25$ rad

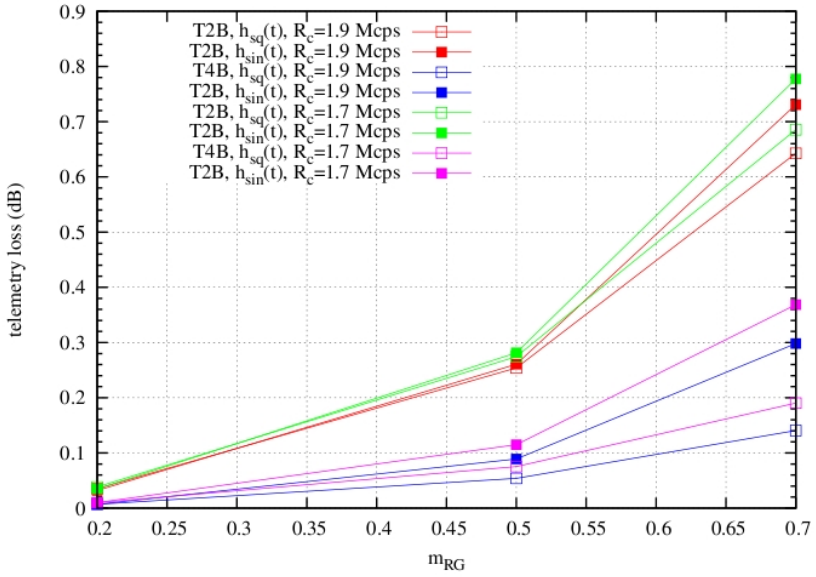

Figure 2-32: Downlink Telemetry Losses (dB) with Respect to m_{RG}, for $m_{TM}=1.25$ rad, and Chip Rates 1.9 Mc/s and 1.7 Mc/s

3 PN TRANSPARENT RANGING SYSTEMS

3.1 INTRODUCTION

Transparent PN ranging is considered attractive in presence of good link margin (e.g., near-Earth applications) or when very accurate ranging is not needed.

The transparent ranging performances are provided, mainly making reference to the equation derived for the regenerative case and in general still applicable. Indeed the expressions derived for code acquisition and tracking (ranging error) are the same or easily derived by them. The substantial difference with respect to the regenerative approach is relevant to the on-board processing and in particular to the possible distortions due to the on-board ranging channel (i.e., amplitude ripple and phase linearity) in the turnaround process. For the transparent ranging channel a description is reported in reference [8] including the specification of the different building blocks and the definition of the non-linearities.

It is worth to underline that, as for the sequential ranging scheme, also the delay stability versus input power, frequency shift and temperature plays a crucial role in the ranging performances and orbit determination process.

3.2 THE SELECTED SEQUENCE T2B

For transparent PN ranging, the uplink processes at the ground station are exactly the same as in the regenerative ranging case. However, in transparent PN ranging the spacecraft does not attempt to acquire the PN ranging sequence; instead, as in the conventional transparent ranging system (also indicated as sequential ranging), it phase modulates the uplink ranging signal as received onto the downlink without further processing. The ground station receiver demodulates the downlink signal and performs the PN ranging correlation in the same manner as for regenerative ranging. Because the uplink noise is re-modulated onto the downlink, the transparent ranging accuracy will generally not be as accurate as with regenerative ranging. The primary advantage is that transparent ranging requires less processing in the on-board transponder, reducing the complexity.

The sequence T2B, already recommended for use with a regenerative channel mainly to cover low SNR conditions, is the sequence selected for transparent channel applications.

3.3 COMPARISON WITH THE REGENERATIVE CASE

3.3.1 STATION PROCESSING: ACQUISITION AND TRACKING

At the ground station, the same processing as in the regenerative case can be performed: the receiver demodulates the downlink signal, recovers the chip-rate and performs the correlation against the probing sequences for acquiring the T2B sequence, employing a full parallel approach. So the analysis for the acquisition performances reported in 2.6 for the regenerative case is still valid. In this case, the Blue Book specifies the acquisition time at 10

dBHz, which gives a theoretical acquisition time of 26.2 s, which is a factor of 100 larger than the transparent case.

Also the tracking performances (in terms of jitter) can be derived from the same expressions evaluated for the regenerative ranging. In particular for the closed loop case (based on CTL) the analysis reported in 2.5 is still valid, while for the open loop architecture the results of 2.7.2 are applicable. Of course the end-to-end performances analysis of 2.7.3 is not applicable anymore since the on-board contribution to the tracking jitter disappears. Table 3-1 show the result with the same conditions indicated in the Blue Book (reference [1]):

– B_L=1 Hz (or T=0.5 s);

– Chip rate F_c = 2.068 Mchip/s; f_{RC}= F_c/2;

– P_R/N_0 =10 dBHz.

Table 3-1: Station Ranging Jitter Performances

Sequence	$\sigma_{Range\_CTL\_sine\_sq}$	$\sigma_{Range\_OL\_sine\_sine}$
T2B	13 m	11.7 m

It is worth to underline that the above results for station acquisition and performances are based on theoretical evaluations assuming an ideal on-board turnaround operation (with no impacts due to non-linearity).

3.3.2 ON-BOARD PROCESSING

The theoretical acquisition performances derived in the previous subsection and obtained using the same equations derived for the regenerative case can be affected by the impacts due to the on-board ranging processing, in particular in-band ripple and phase linearity. Analysis was done in order to define requirements for:

– the channel non-linearities (in-band group delay variations and gain flatness);

– the 3 dB bandwidth;

– and the noise bandwidth.

The analysis is performed in a parametric way considering:

– different high cut-off frequencies;

– the presence or not of a TC echo rejection filter (low cut-off frequency).

It is shown in references [8], [11] and [12] that:

- A pure low-pass channel offers better acquisition performances compared to a channel with a high pass filter to remove the TC.
- In case of a high pass filter with cut-off at around 350 kHz, calculated acquisition times for F_c = 3 Mchip/s increased by about 50%. At very low P_R/N_0, the effect is that the acquisition time becomes impractically long.
- To keep the on-ground PN sequence acquisition close to the theoretical value, a wideband channel is desirable.
- The one-sided bandwidth has to be at least 1.5*F_c wide for a maximum 10% increase of acquisition time.

4 PN RANGING VIA NON-COHERENT TRANSPONDERS

4.1 GENERAL

For missions that desire to range using a transceiver or a non-coherent transponder and do not require high accuracy ranging, it is possible to perform two-way non-coherent ranging. This technique has the advantage that it can allow for simpler hardware onboard the spacecraft. It can be applied to either transparent or regenerative ranging.

With two-way non-coherent ranging, the on-board processing of the uplink signal is identical to the coherent ranging described in previous subsections. The spacecraft either phase modulates the noisy received uplink PN ranging signal onto the downlink carrier (in the transparent ranging case), or acquires the PN ranging sequence and regenerates the uplink ranging signal as described in 2.4 (in the regenerative ranging case). However, because the downlink carrier frequency is referenced to an onboard oscillator rather than the uplink carrier, the ground station will not be able to perform carrier Doppler pre-steering of the ranging signal. This is because the received chip rate has Doppler contributions from both the uplink and downlink, while the received carrier frequency only has Doppler contribution from the downlink plus a frequency error component due to the onboard oscillator. Doppler pre-steering requires that the received carrier Doppler and chip rate Doppler be matched.

When using non-coherent ranging and an open loop receiver at the station, there will generally be a chip rate mismatch between the received PN code and the local model correlated against at the ground station. This is due to uncompensated Doppler. The difference in the chip rates will cause the ranging correlation to be degraded, and introduce a range bias in the measurement. If the spacecraft trajectory is well known, then the uplink frequency and chip rate can be adjusted to minimize the Doppler seen at the spacecraft.

Additionally, there is also a chip rate mismatch due to the spacecraft oscillator frequency error component. This can be mitigated, but in general not entirely removed, by adjusting the uplink frequency and chip rate to compensate for the spacecraft oscillator frequency drift in addition to the uplink Doppler. Another solution would be to use a Ultra-Stable Oscillator (USO) as a reference for the downlink carrier and PN chip rate onboard the spacecraft.

4.2 GROUND STATION OPEN LOOP RECEIVER

For the open loop model of the ground station receiver, the range clock mismatch between the received PN code and the local model has two primary effects. The first effect is a reduction in correlation amplitude, which in turn reduces the ranging SNR and makes the range measurement noisier. The reduction in correlation amplitude, A_c, is given by reference [3]:

$$A_c = \left| \frac{\sin(\pi \Delta f_{chip} T)}{\pi \Delta f_{chip} T} \right|$$

where Δf_{chip} is the frequency difference between the received chip rate and the local model (the chip rate is twice the range clock frequency), and T is the integration time. The reduction in correlation amplitude reduces the ranging SNR and increases the jitter due to thermal noise and the acquisition time.

The second effect is a range bias introduced because of the frequency mismatch. The difference in frequency between the local model and the received range clock causes the phase difference between them to drift during the measurement interval. Provided that the range measurement is referenced to the start of the integration interval instead of the middle, the range error is equal to one-half the total drift during the integration time, T, as follows reference [3]:

$$Range\ bias = \frac{c\Delta f_{chip} T}{4 f_{chip}}$$

where Δf_{chip} is the difference in frequency between the received chip rate and the local chip rate. The frequency error will in general have contributions due to both spacecraft oscillator frequency drift and imperfect uplink Doppler predicts. The range bias error is proportional to the integration time for a given chip rate difference. Thus for non-coherent ranging measurements, it is preferable to use the shortest integration time allowed by the thermal noise constraint.

4.3 GROUND STATION CLOSED-LOOP RECEIVER

For the closed-loop model of the ground station ranging receiver, the CTL bandwidth must be made wide enough to track the changes in chip rate caused by on-board oscillator drift and uncompensated Doppler. This will limit the jitter performance as described by equations in 2.7 (for the regenerative case) and 3.3 (for the transparent ranging case). In addition, there will be a range bias as described by the equation in the previous subsection.